



Low paleolatitude of the Carajás Basin at ~2.75 Ga: Paleomagnetic evidence from basaltic flows in Amazonia

Pedro L.G. Martins^{a,*}, Catarina L.B. Toledo^a, Adalene M. Silva^a, Paul Y.J. Antonio^b, Farid Chemale Jr.^c, Luciano M. Assis^d, Ricardo I.F. Trindade^b

^a Universidade de Brasília, Instituto de Geociências, 70910-900 Brasília, DF, Brazil

^b Instituto de Astronomia, Geofísica e Ciências Atmosféricas, Universidade de São Paulo, 05508-090 São Paulo, SP, Brazil

^c Universidade do Vale do Rio dos Sinos, Departamento de Geologia, 93022-000 São Leopoldo, RS, Brazil

^d Diretoria de Geociências, Planejamento de longo prazo e Uso futuro, Vale S.A., Mina de Águas Claras, Av. Dr. Marco Paulo Simon Jardim, 3580 Nova Lima, MG, Brazil

ARTICLE INFO

Keywords:

Amazonia
Paleomagnetism
Superia
Carajás Province

ABSTRACT

Establishing the positions of continents during the initial stages of Earth's evolution is one of the most important challenges in geosciences today. This challenge is mainly due to the severe limitations in obtaining geological and/or geophysical data from early Earth time, particularly robust paleomagnetic data. Here, we report the first paleomagnetic data from an Archean block in the Amazonian craton, the Carajás Province, for ~2.76–2.74 billion years ago (Ga), when extensive dominantly mafic volcanism (Parauapebas Formation) covered an area of ~18,000 km². The paleomagnetic investigation was conducted on fresh drill cores drilled into the Carajás iron ore mine and cutting across the Parauapebas Formation. After rotating the drill core segments to geographic coordinates using the viscous magnetic component, two characteristic components, Carajás 1 and 2 (C1 and C2) were identified and further used to calculate paleomagnetic poles: C1 (~2759 Ma; 40.5°E, -44.6°S, N = 5, A₉₅ = 6.5°, K = 18.5) and C2 (~2749 Ma; 342.4°E, -54.3°S, N = 28, A₉₅ = 14.8°, K = 27.8). Pole C2 is based on a bigger number of sites, passes a reversal test and is considered robust. A baked contact test was attempted for this component, but it is not conclusive. Our results, integrated with geological evidence reveals that the Carajás block occupied low latitudes at the time, and could have been part of the Superia supercraton during the Neoproterozoic (~2.75 Ga) at equatorial latitudes. Finally, a consistent succession of six magnetic reversal events was identified in the lava flow sequence from the Parauapebas Formation, pointing to an already dynamic geodynamo pre-2.7 Ga.

1. Introduction

During the Archean, the first continents were formed and their remnants are now dispersed around the world. At present, there are approximately thirty-five of these ancient fragments of crust preserved globally (e.g., Bleeker, 2003). These ancient cratons form the nucleus of the present-day continents, and are a 'window' back into the environments of the early Earth. The Archean cratons stabilized at different times worldwide from 3.1 to 2.5 Ga, with a peak in cratonization heralding the transition from a mafic to a more evolved intermediate composition (Bleeker, 2003; Cawood et al., 2018; Hawkesworth et al., 2020). Additionally, records of Earth's primitive atmosphere and oceans emerge in the earliest to latest Archean, and evidence of the earliest primitive life forms appears in rocks about these old times (e.g.,

Planavsky et al., 2021). Crust–mantle interactions also seem became significantly more prominent towards the end of the Archean, reflecting a significant change in mantle dynamics and plate tectonics during the Neoproterozoic (Halla et al., 2017; Gerya, 2019; Palin et al., 2020; Windley et al., 2021). Establishing the positions of continents at this time, when the continental configuration is yet poorly known and intensely debated, is one of the most important tasks in deciphering the geological evolution of the planet at its youth. The first-order question to answer is whether the Archean continental blocks were amalgamated into a single, large supercontinent, putatively named "Kenorland" (Williams et al., 1991), or whether they were dispersed into several smaller "supercratons" such as Superia, Zimgarn, Sclavia, and Vaalbara (e.g., Bleeker, 2003; Smirnov et al., 2013). In that sense, paleogeographic reconstructions are a key discriminant between these hypotheses,

* Corresponding author.

E-mail address: plgmartins@gmail.com (P.L.G. Martins).

<https://doi.org/10.1016/j.precamres.2021.106411>

Received 20 April 2021; Received in revised form 9 September 2021; Accepted 9 September 2021

Available online 24 September 2021

0301-9268/© 2021 Elsevier B.V. All rights reserved.

providing a clearer picture of the ancestral landmass(es) configuration. Unlike Proterozoic supercontinents (Rodinia and Columbia), the paleogeography for the late Archean cratons is not so clear, owing to the general paucity of paleomagnetic data from most cratons (Buchan et al., 2000; Pesonen et al., 2003). Nevertheless, particularly during the Neoproterozoic Era, the relative positions of cratons are becoming tractable by the increasing numbers of refined paleomagnetic data and geochronologic studies (e.g., de Kock et al., 2009; Denyszyn et al. 2013; Smirnov et al., 2013; Salminen et al., 2019; Liu et al., 2021).

South American cratons, such as São Francisco and Amazonian, have been absent from most of the Archean supercraton reconstructions. Recently, Salminen et al. (2019), based on paleomagnetic data and comparison of magmatic barcodes, demonstrated that the Uauá block, a fragment of the São Francisco craton, could have been part of a much larger supercraton named Supervaalbara by Gumsley (2017) constrained at 2.43 Ga. Meanwhile, the paleogeography of the Amazonian Craton (Fig. 1A), one of the largest cratonic areas in the world (~5,600,000 km²; Almeida et al., 1981), remains a challenging task especially during Archean-Paleoproterozoic times, being one of the least studied Archean cratons (D'Agrella-Filho et al., 2016).

Here, we focus on the paleomagnetic record of an Archean block in the Amazonian craton, the Carajás Province (Fig. 1) for the ~2.76–2.74 Ga interval, when extensive volcanism, dominantly mafic, covered an area of approximately 18,000 km² (Macambira, 2003). This volcanism produced the Parauapebas Formation, the lowermost unit of the Neoproterozoic volcanic-sedimentary sequence of the Grão-Pará Group (Vasquez et al., 2008; Martins et al., 2017). We report new paleomagnetic data for basaltic lava flows from two well-preserved deep drill cores sampled from the Carajás Basin in the northern Carajás Province. Our goal is to provide the first paleogeographic constraints for this Archean block, yielding a paleolatitude estimate for the block and discussing its affiliation to previously proposed Archean cratonic assemblies (e.g., Williams et al., 1991; Bleeker, 2003; Bleeker and Ernst 2006; de Kock et al., 2009; Gumsley et al., 2017; Salminen et al., 2019; Liu et al., 2021). Furthermore, the thick sequence of basalts in the Carajás Basin has a good potential to provide evidence for geomagnetic reversals across the succession.

2. Geological setting

The tectonic framework of the Amazonian Craton essentially consists of one ancient nucleus, the Central Amazonia Province (>2.60 Ga), and adjacent Paleo- and Mesoproterozoic provinces (see Teixeira et al., 2019 for review). The eastern portion of the Central Amazonia Province (Fig. 1A) is comprised of the Carajás Province, which is renowned for hosting several world-class mineral deposits of Fe and Cu-Au, as well as Mn and Ni mines (Vasquez et al., 2008; Moreto et al., 2015). The Carajás Province (Carajás block) is divided in two domains, the northern Carajás and the southern Rio Maria (Fig. 1B) (Vasquez et al., 2008). A broad E-W striking shear zone (known as the “Transition” subdomain), mostly within the Carajás Domain, occurs between the volcano-sedimentary Carajás Basin and rocks of the Rio Maria Domain (Fig. 1B) (Dall’Agnol et al., 2006; Feio et al., 2013). The Rio Maria Domain is a typical granite-greenstone terrane, mainly composed of tonalite-trondhjemite–granodiorite (TTG) associations, surrounded by greenstone belts, with formation ages between ca. 3.00–2.85 Ga (e.g., Almeida et al., 2011, 2013 and references therein).

Apart from the strongly deformed granitoids and gneissic rocks of the Transition subdomain, the Carajás Domain is composed essentially of the Carajás Basin (Vasquez et al., 2008; Fig. 1B; Fig. 2), also known as the central sigmoid of Carajás (Holdsworth and Pinheiro, 2000). The basement of the Carajás Basin comprises 2.98–2.86 Ga Mesoproterozoic granitoids of the Xingu Complex (similar in age and lithological content to the Transitional subdomain; Machado et al., 1991). The main assemblages of the Carajás Basin are of Neoproterozoic age and it is commonly segmented into the lowermost volcanic-sedimentary Grão-Pará Group (2.76–2.73 Ga; Fig. 2; Fig. 3) overlain by sedimentary rocks of the ca. 2.68–2.06 Ga Serra Sul and Águas Claras formations (Araújo and Nogueira, 2019; Araújo Filho et al., 2020; Rossignol et al., 2020) (Fig. 2; Fig. 3).

The Neoproterozoic Grão-Pará Group (2.76–2.73 Ga) is the main volcano-sedimentary sequence of the Carajás Basin, and is approximately 260 km long and 70 km wide, with its rocks covering an area of approximately 18,000 km² (Macambira, 2003; Vasquez et al., 2008; Fig. 2). For the Grão-Pará Group stratigraphy, we follow the

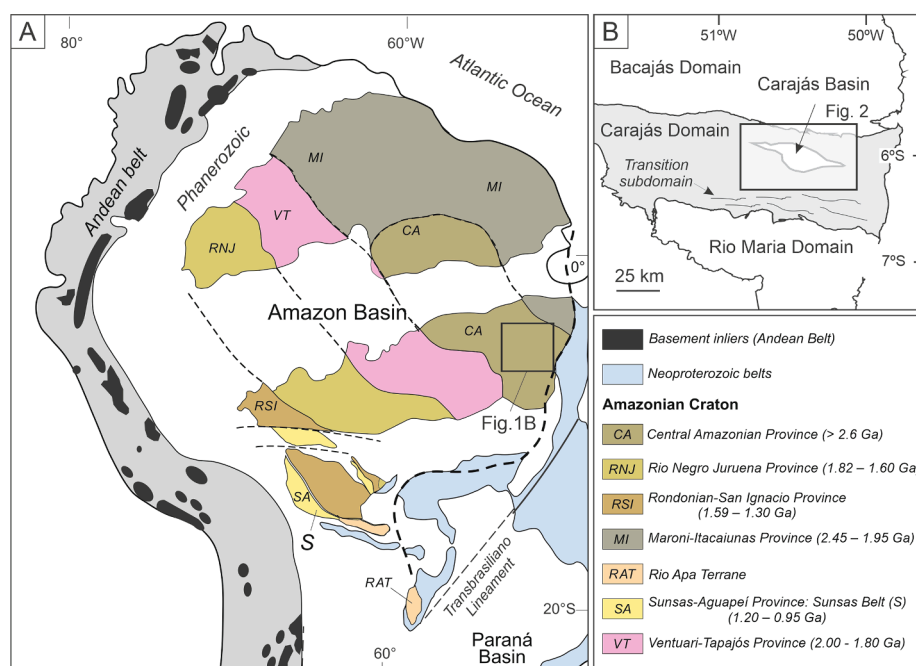


Fig. 1. A) Amazonian Craton and its geologic/geochronological provinces (adapted from Cordani and Teixeira 2007; Teixeira et al., 2019); B) Carajás province map showing the location of the Carajás Basin in the Carajás Domain (from Araújo Filho et al., 2020); the black rectangle indicates the approximate location of Carajás Basin (Fig. 2).

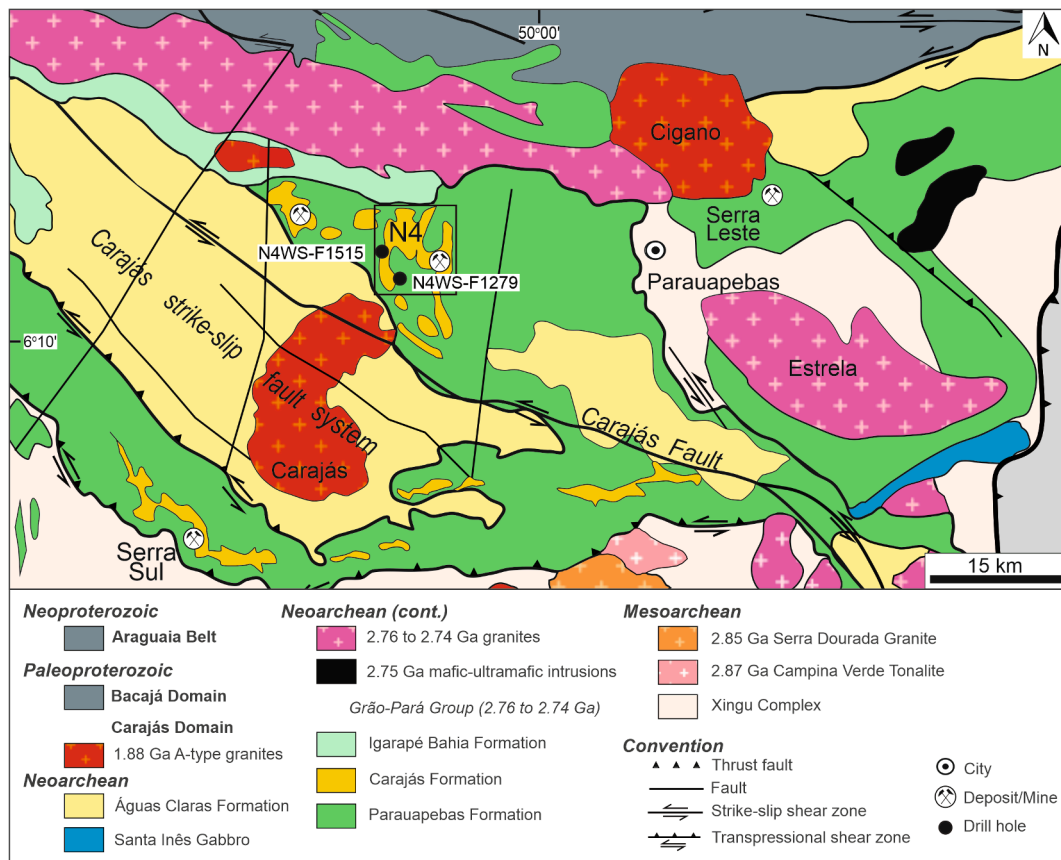


Fig. 2. Simplified geological map of the northeastern part of Carajás Province (modified from Vasquez et al., 2008) showing the location of drill cores (black dots inside black rectangle).

stratigraphic framework proposed by Araújo and Nogueira (2019) and Araújo Filho et al. (2020), who defined the group from the base to the top to be composed of the following units: Parauapebas, Carajás, and

Igarapé Bahia formations (see Fig. 3). The basal Parauapebas Formation is the focus of our paleomagnetic study. It consists of basalts and basaltic andesites with minor pyroclastic rocks and rhyolites (Gibbs et al., 1986;

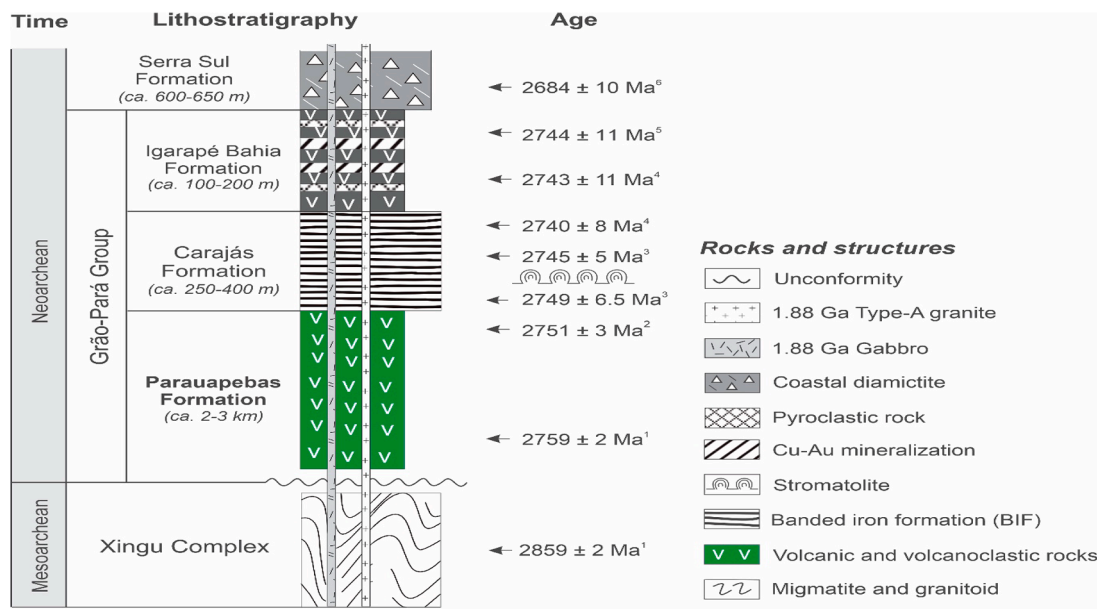


Fig. 3. Stratigraphy of the basal part from Carajás Basin with indication of geochronological constraints (adapted from Araújo and Nogueira, 2019; Araújo Filho et al., 2020). Geochronological data compiled from: 1—Machado et al. (1991); 2—Krymsky et al., 2002; 3—Martins et al. (2017); 4—Trendall et al. (1998); 5—Galarza et al. (2008); 6—Maximum depositional age from Rossignol et al. (2020). The time column was adapted from the International Chronostratigraphic Chart v2020/01 (Cohen et al., 2013).

Martins et al., 2017; Figueiredo e Silva et al., 2020), and is usually considered to be the result of intraplate rifting of older continental crust (e.g., Gibbs et al., 1986; Olszewski et al., 1989; Martins et al., 2017; Tavares et al., 2018; Teixeira et al., 2021). However, a subduction-related setting has also been suggested (e.g., Meirelles and Dardenne, 1991; Teixeira and Egger, 1994; Zucchetti, 2007; Figueiredo e Silva et al., 2020). The age of this extensive volcanism is well constrained between 2759 ± 2 Ma and 2745 ± 5 Ma, using U-Pb analyses of zircon from rhyolites and basalts of the Parauapebas Formation (e.g., Olszewski et al., 1989; Machado et al., 1991; Trendall et al., 1998; Martins et al., 2017).

The Carajás Formation consists of by layers and discontinuous lenses of banded iron formations (jaspilites) and iron ore, intruded by sills and mafic dykes. The base of the Carajás Formation is interlayered with volcanic rocks of the underlying Parauapebas Formation (Gibbs et al., 1986; Martins et al., 2017), showing a gradual and conformable contact that reflects the contemporaneity of the formations. The BIF sequence is overlain by volcanic and volcanoclastic rocks, as well as subordinate deep-water marine turbidite strata belonging to the Igarapé Bahia Formation (Tallarico et al., 2005; Dreher et al., 2008; Galarza et al., 2008; Fig. 3). Existing U-Pb zircon data constrain the age of the volcanic rocks of the Igarapé Bahia Formation at 2743 ± 11 Ma (Trendall et al., 1998).

The most conspicuous structural feature of the Carajás Basin is an S-shaped syncline-anticline pair (Rosière et al., 2006), the Carajás fold, that is partially disrupted by the Carajás strike-slip system (Fig. 2). The latter divides the Serra dos Carajás in two main blocks, named Serra Norte and Serra Sul. We sampled two exceptionally well-preserved, deep drill cores of the Serra Norte region (N4 deposit) for paleomagnetism.

Forty-five geochemical analyses of Parauapebas basaltic flows are reported by Martins et al. (2017), including sampling localities and brief descriptions. Several of these flows were sampled for paleomagnetism in this study (e.g., N4WS-F1279). These geochemical investigations on basaltic rocks of the Parauapebas Formation show 51.12–55.26 wt% SiO₂, 0.69–0.92 wt% TiO₂, 7.02–12.35 wt% FeO, and MgO ranging from 4.38 to 7.38 wt%. Moreover, the Parauapebas flows are sub-alkaline, plot in the transitional and calc-alkaline fields, and show either arc-like trace element patterns or patterns similar to those of the upper continental crust. Geochemically, this is apparent in their LILE and LREE enrichment and Nb and Ti depletion, supporting the idea that the basaltic rocks from Parauapebas Formation are derived from the sub-continental lithospheric mantle affected by upper continental crustal contamination (Martins et al., 2017).

3. Sampling and analytical procedures

3.1. Sampling

Due to the challenging conditions of outcrops in the densely forested Amazonia, well-preserved, unweathered rocks are difficult to observe in the Carajás Basin. Therefore, we must rely on mining pits and drilled cores to obtain fresh samples. Rock samples were collected from two well-preserved deep drill cores (N4WS-F1279 and N4WS-F1515) of the N4WS deposit region, in the northern part of the Carajás Basin (Fig. 2; S1). The drill holes are roughly aligned in a NW-SE section (Supplementary data, Fig. S1; S2). These fresh cores were selected for their well-preserved succession of basaltic flows, and apparent absence of post-depositional deformation and high-grade metamorphism (Fig. 5; Fig. 6).

The core samples were obtained at the Vale core library in Serra dos Carajás, Pará. At the N4WS-F1279 drill hole (Lat/Long coordinate: $6^{\circ} 06' 10''$ S, $50^{\circ} 10' 49''$ W, WGS84), a continuous ~ 350 m long core was obtained from the Parauapebas Formation, composed of basaltic rocks (Fig. 4; S2). Meanwhile, the N4WS-F1515 drill hole (Lat/Long coordinate: $6^{\circ} 04' 55''$ S, $50^{\circ} 11' 39''$ W, WGS84) is stratigraphically superjacent (Fig. 4) and the samples were obtained through a total core length of 360 m (200–560 m depth). The core is divided into mafic volcanic/subvolcanic rocks and banded iron formations (BIFs) corresponding to

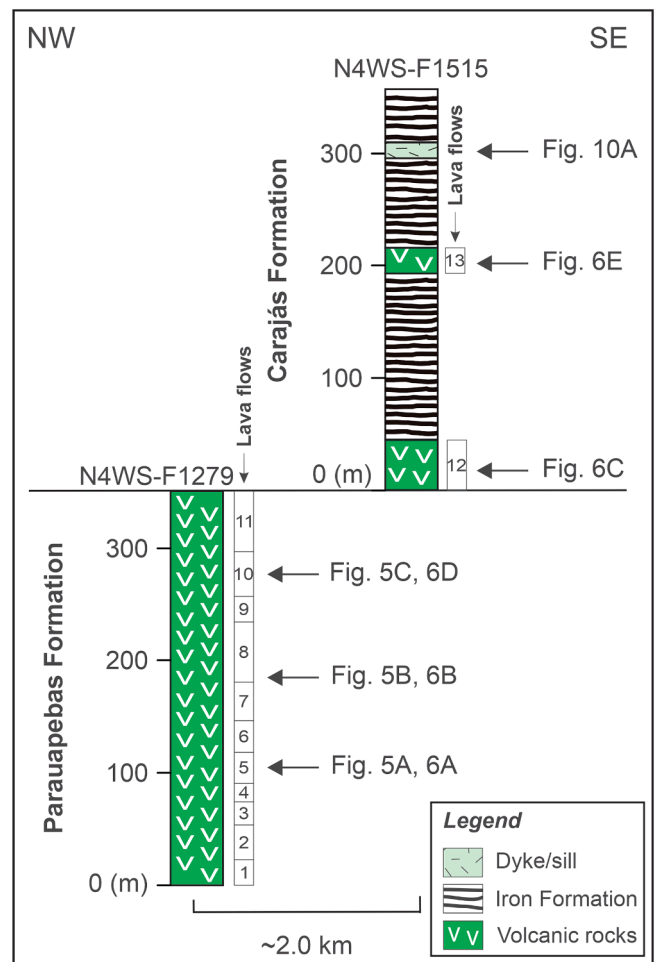


Fig. 4. Stratigraphic correlation between studied drill cores from the N4WS deposit running through the Parauapebas and Carajás formations. Numbers and letters to right of the columns correspond to photos in Figs. 5, 6, and 10.

the Parauapebas and the Carajás formations (Fig. 4; S2).

The drill holes were performed for N4WS-F1279 with a plunge angle of 81° toward 94° azimuth and for N4WS-F1515 with a plunge of 75.8° toward 262° azimuth, in both cases nearly perpendicular to the bedding in each sector (Fig. S2), enabling the orientation of the cores. The orientation of the cores was confirmed at 10 m intervals. It is important to stress that the strike and dip of the beds remained constant from the surface to the bottom of the drilled core from the N4WS body. The constant strike and dip were confirmed by a field survey of surface outcrop. The orientation of the Grão-Pará Group at N4WS-F1279 strikes 184° and dips 9° to the West. At N4WS-F1515 core the bedding is opposed and strikes 352° and dips 14.2° to the East (Fig. S1; S2).

3.2. Paleomagnetism and rock magnetism

We obtained paleomagnetic results on 33 pieces of drill core (~ 15 cm long and 8 cm in diameter) distributed along 13 lava flows (Fig. 4) at different heights across the stratigraphy of the Parauapebas and Carajás formations. A total of 27 pieces of drill core were collected from drill core N4WS-F1279 and 6 from drill core N4WS-F1515 (Fig. S2). Each length of core was considered as an independent record of the geomagnetic field, and were thus treated as a single paleomagnetic site. These pieces of core correspond to the working half of the 8-cm diameter drill cores. These half drill cores were then plugged perpendicular to the length of the core into cylindrical samples of 2.54 cm in diameter. Each sample provided a single specimen for measurements with a typical size



Fig. 5. Macroscopic aspects of the basalts from Parauapebas Formation: A) and B) Overview of sampled cores showing the basaltic lava flow, characterized by massive texture on the bottom and amygdaloidal and spilitization zones at the top (increasing depth from left to right); C) Amygdaloidal zone; amygdules are mainly filled with calcite and chlorite.

Table 1

Paleomagnetic results for 2.75 Ga Carajás basalts and associated baked contact tests. Drill hole position represents the location of the samples in the Fig. 7.

Site	Lithology	Flow	Depth (m)	Stratigraphic height (m)	Characteristic remanent magnetization				VGP		
					n/N	Dec (°)	Inc (°)	k	α95 (°)	Plat (°N)	Plong (°E)
N4WS-F1279 (6.065°S / 50.184°W; strike: 184° and dip: 9°)											
F1279-E	Basalt	2	317.30	52.20	5/6	162.5	53.6	65.4	4.8	-57.6	337.5
F1279-F	Basalt	2	320.50	49.00	11/12	132.7	39.5	53.6	10.8	-41.6	15.1
F1279-G	Basalt	2	334.50	35.00	6/9	175.3	53.8	94.9	9.5	-61.4	317.9
F1279-ZD	Basalt	1	355.50	14.00	16/17	342.6	-62.5	28.5	7.1	-49.3	329.1
F1279-ZE	Basalt	1	362.50	7.00	4/5	336.9	-56.1	30.6	16.9	-52.9	341.2
<i>Mean sites C1</i>					5	156.4	54.1	38.4	12.5	-54.3	342.4
<i>Mean sites C1 rotated to PDF</i>					5	174.9	54.1	38.4	12.5	-61.0	318.5
F1279-A	Basalt	11	22.30	347.20	12/13	146.1	4.6	43	6.7	-56	44.7
F1279-B	Basalt	11	29.20	340.30	8/9	150.8	0.1	93.5	5.8	-60.2	50.5
F1279-C	Basalt	11	35.45	334.05	4/4	132	3.9	36.3	15.5	-42	42.7
F1279-H	Basalt	10	71.40	298.10	9/9	116	-4.9	96.6	6.3	-25.5	45.5
F1279-I	Basalt	10	74.80	294.70	8/11	154.5	-7.2	108.5	6.9	-62.7	60
F1279-J	Basalt	10	84.50	285.00	15/18	144.8	18	33.4	5.3	-55	32.4
F1279-L	Basalt	9	104.3	265.20	13/15	148.6	3.1	28.1	5.3	-58.4	46.8
F1279-M	Basalt	9	105.00	264.50	5/5	152.2	5.1	30.4	6.7	-62.1	45.9
F1279-O	Basalt	8	131.10	238.40	6/7	115.6	13.2	55.3	8.1	1.7	32.9
F1279-P	Basalt	8	142.65	226.85	8/11	313.7	-14	40.3	14.5	-16.3	34.2
F1279-Q	Basalt	7	173.35	196.15	5/5	332.4	-18.3	20.3	9.1	-34.9	32.6
F1279-R	Basalt	7	185.30	184.20	4/5	143.4	20.3	36.7	9.4	-53.5	30.4
F1279-S	Basalt	7	198.40	171.10	10/15	130.3	-8.1	36.3	17.4	-39.3	50.2
F1279-T	Basalt	6	225.55	143.95	11/14	103.9	-13.6	24.7	13.9	14.7	45.4
F1279-U	Basalt	6	244.10	125.40	4/6	122.6	-17.2	197.5	8.5	-30.9	53.9
F1279-V	Basalt	5	249.15	120.35	6/6	302.5	-17.4	26.2	9.4	-5.4	31.4
F1279-X	Basalt	5	266.60	102.90	13/15	294.6	8.2	39.5	6.6	3.8	43.6
F1279-Y	Basalt	4	278.60	90.90	14/14	129.8	-13.3	95.1	13.3	-38.3	53.4
F1279-Z	Basalt	4	287.55	81.95	6/6	134.3	7.9	62	6.8	-16.6	37.5
F1279-ZB	Basalt	3	294.50	75.00	5/5	115.6	-20.8	81.5	4.1	3.5	50.3
F1279-D	Basalt	3	301.60	67.90	8/9	315.4	-31.9	27.2	8.6	-18.4	23.6
F1279-ZC	Basalt	3	311.70	57.80	15/15	162.7	22.8	66.2	8.5	-72	19.9
N4WS-F1515 (6.082°S / 50.195°W; strike: 352.1° and dip: 14.2°)											
F1515-E-D*	Basalt	-	211.45	728.55	4/4	140.7	39.5	G.C.	10.3	-48.7	12.4
F1515-E-B*	BIF	-	211.45	728.55	4/8	151.5	39.4	G.C.	21.9	-58.1	6.4
F1515-M	Basalt	13	328.40	611.60	18/18	301	-31.8	65.9	4.3	-31.4	23.3
F1515-Y	Basalt	12	522.45	417.55	9/9	289.8	16.9	70.9	6.5	-18.5	51
F1515-Z	Basalt	12	523.90	416.10	14/14	301.7	22.6	25.2	8.4	-29.3	57
F1515-ZB	Basalt	12	537.75	402.25	14/15	159	26.2	54.1	5.5	-67.9	17.7
<i>Mean sites C2</i>					28	134.3	6.8	11.3	8.5	-44.6	40.5
<i>Mean sites C2 rotated to PDF</i>					28	152.8	6.8	11.3	8.5	-62.77	44.16

n/N = number of analyzed samples/number of samples used in the mean; Dec. = declination; Inc. = inclination; α95 and k = Fisher's confidence cone and precision parameter (Fisher, 1953); G.C. –Great circles analysis; VGP – Virtual Geomagnetic Pole; P. Long – Paleolongitude; P. Lat – Paleolatitude. * = Samples from baked contact test.

of 2.20×2.54 cm. From the 33 fragments of drill core studied, we obtained a total of 318 standard specimens for paleomagnetic analyses (Table 1).

Preparation and magnetic demagnetization of the specimens were performed in the Paleomagnetic Laboratory of the Instituto de Astronomia e Geofísica of the University of São Paulo (USPMag, Brazil). At least four specimens from each core sample were subjected to detailed stepwise alternating magnetic field (AF) and thermal demagnetization techniques to isolate the characteristic remanent magnetization (ChRM). Steps of 2.5 mT (up to 15 mT) and 5 mT (15–100 mT) were selected for AF demagnetization. Devices used were a tumbler Molspin AF demagnetizer coupled to a JR-6A spinner magnetometer (AGICO, Czech Republic); an automated three-axis AF demagnetizer coupled a horizontal 2G-Enterprises™ DC-SQUID magnetometer or to a vertical

2G-Enterprises™ DC-SQUID magnetometer with RAPID sample changer (Kirschvink et al., 2008). Thermal demagnetization was performed using a Magnetic Measurements TD-48 furnace in steps of 50 °C (from 150 °C up to 500 °C) and 20 °C (from 500 °C up to 600 °C/700 °C). Magnetic components for each specimen were identified in orthogonal plots (Zijderveld, 1967), and calculated using principal component analysis (Kirschvink, 1980). At least six steps were considered for computing the magnetic components without anchoring the directions. Line-fits were filtered using an upper limit of 8° for maximum angular deviation (MAD). For some sites, remagnetization great circles analysis (Halls, 1978) was also employed to determine high coercivity/high-blocking temperature components.

Site-mean paleomagnetic directions and paleomagnetic poles were calculated using Fisher statistics (Fisher, 1953). A site-mean direction

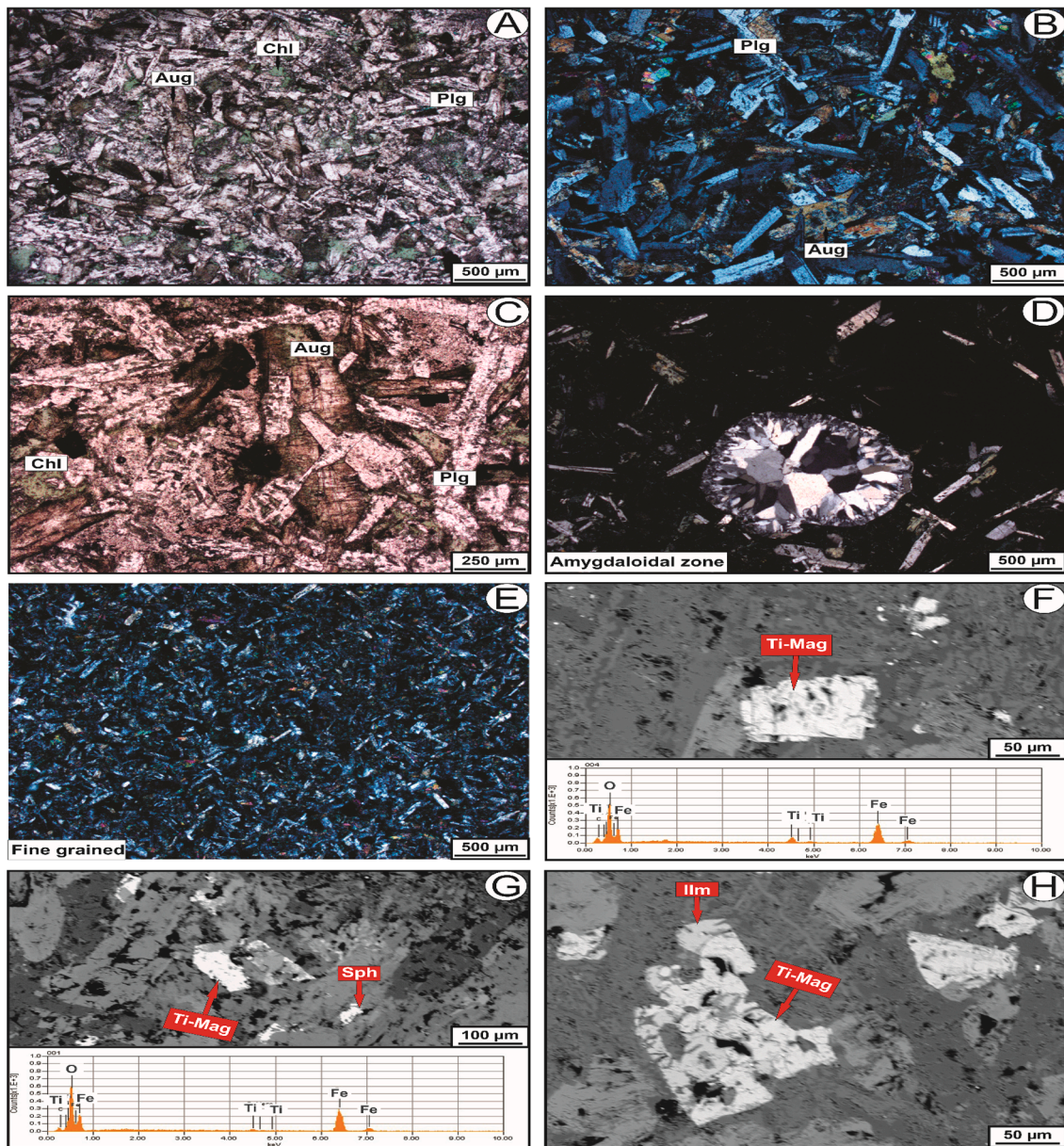


Fig. 6. Photomicrographs of representative basalts of Parauapebas Formation: A) Basalt exhibits preserved primary igneous texture (intergranular/interstitial); B) Intergranular texture; C) Primary mineral assemblage still preserved, mainly composed by plagioclase and augite; D) Amygdale with subcircular form filled with quartz in a fine-grained groundmass of augite, plagioclase and glass (replaced by chlorite); E) Fine-grained basalt; F) and G) Backscatter electron image of representative basaltic sample, showing primary Fe-Ti oxides and EDS spectra associated titanomagnetite with ilmenite alteration; H) Backscatter electron image showing primary titanomagnetite with ilmenite alteration; Mineral abbreviations: (Aug) augite, (Chl) chlorite, (Ilm) ilmenite, (Plg) plagioclase, (Sph) sphalerite, and (Ti-Mag) titanomagnetite.

was accepted if calculated from at least three individual specimen directions with an associated 95% confidence circle (α_{95}) not exceeding 20° . Paleomagnetic data processing was carried out using Paleomac software (Cogné, 2003). The GPlates software was used for paleogeographic reconstructions (Müller et al., 2018). In addition, the magnetic mineralogy of each site was investigated to determine the carriers of magnetic remanence. These analyses were performed at the Laboratory of Geochronological, Geodynamic and Environmental Studies (LabGEO) of Instituto Oceanográfico da Universidade de São Paulo. Magnetic hysteresis and Isothermal remanent magnetization (IRM) measurements were performed at room temperature by using a MicroMag-VSM, Model 3900 (Princeton Measurements Corporation, USA) with a maximum magnetic field of 1 T. The thermomagnetic curves were measured on powdered samples during continuous heating to 700°C and cooling to room temperature by using a CS-4 apparatus coupled to the KLY-4S Kappabridge instrument (AGICO, Czech Republic).

A total of 24 thin sections were also examined using reflected and transmitted light microscopy. In addition, Scanning Electron Microscopy (SEM) analysis and X-ray energy dispersive spectroscopy (EDS) using a JEOL JXA-8230 SuperProbe at the Electron Microprobe Laboratory of the University of Brasília (Brazil) was used to constrain the nature and textures associated with the magnetic carriers.

4. Field aspects and petrography

The Parauapebas Formation in the studied drill cores consists of extensive successions of massive or amygdaloidal lava flows with at least 370 m in cumulative thickness. The basaltic lavas display different textures (amygdaloidal, massive, aphanitic, fine-grained and porphyritic; Figs. 5 and 6). Thirteen lava flows cycles were identified by massive texture at the bottom and amygdaloidal and spilitized (seawater metasomatic alteration) zones at the top (Fig. 5). The base and central portions of each lava flows are massive to coarse-grained, respectively. However, amygdaloidal (Fig. 5C; 5) and spilitized zones are common in the boundary between each lava flow unit (Fig. 5A). Primary mineral assemblages and igneous textures (largely amygdaloidal, intergranular and intersertal and rarely microporphyritic) are preserved (Fig. 5; Fig. 6A-E). The basalts consist predominantly of clinopyroxene (Fig. 6B; C) and plagioclase with minor quartz, K-feldspar, ilmenite, magnetite and rare pyrite. Titanite and zircon are present as accessory minerals. Common alteration in these rocks is the replacement of calcic plagioclase by sodic plagioclase, and the major replacement of glass and augite by chlorite (Fig. 6A). Alteration of both pyroxene, glass and plagioclase has been attributed to seafloor hydrothermal activity (Martins et al., 2017; Figueiredo e Silva et al., 2020).

The Fe-oxides were examined using a Scanning Electron Microscope (SEM) to explore their primary character. Fe-oxides observed in thin section include fine ($>10\ \mu\text{m}$) grains of titanomagnetite (Fig. 6F-H) with typical sizes of 10–150 μm containing ilmenite alteration in some cases (Fig. 6H), and ilmenite. Intergrowth textures with ilmenite exsolutions are generally related to a stable thermoremanent magnetization (Evans and Wayman, 1974). Although, titanomagnetite grains exhibit a small size, it was possible to detect the primary character of octahedral magnetite within a plagioclase crystal (Fig. 6G). Both textures are most likely of magmatic origin (Nesse, 2000). Different types of sulfides (sphalerite, pyrrhotite) are also observed (Fig. 6H). The magnetic mineralogy analyses are discussed further.

5. Paleomagnetic results

In the studied rocks, AF demagnetization was more efficient than thermal demagnetization. In all specimens it is possible to identify a low-coercivity viscous remanent magnetization (VRM) component below 16 mT. This magnetic component was used to rotate the drill core sections to the true North position. We arbitrarily assumed the orientation of VRM coincides with the present-day field (PGF), but rotation the results

to the recent dipolar field is equally valid (Audunsson and Levi, 1989; Rolph et al., 1995; Rapalini et al., 2013). The local declination for the Carajás region is -18.5° . The choice to orient the drill cores based on alignment of the VRM to the PGF is explored in the discussion sections. In Figs. 7, 8 and 9 we show the directions already rotated to the present-day field.

AF demagnetizations for the N4WS-F1279 reveal a ChRM of southeastern direction and low inclination (Fig. 7A, E) or of northwestern direction and low inclination (Fig. 7B, C). The remanence is carried mostly by magnetite as showed by thermal demagnetization with a high blocking temperature ($\sim 540^\circ\text{C}$; Fig. 7D). At the bottom part of the core, from 0 m to 54 m, the inclination values are $>30^\circ$ (Fig. 7F). Specimens from the N4WS-F1515 core show a similar ChRM to that of the top part of N4WS-F1279 with a northwestern direction of low inclination (Fig. 7G, H). The similarity of the ChRM results along the stratigraphy and between the two drill cores after correcting for VRM alignment with PGF is an important local consistency test reinforcing the validity of the reconstructed in-situ sample orientation.

The ChRM direction and latitude of Virtual Geomagnetic Pole (VGP Lat) are plotted along the stratigraphy in Fig. 9 after deleting the samples with $\text{MAD} > 8^\circ$. Whereas the top part of N4WS-F1515 is not well-defined due to the intercalation of BIFs (not sampled), the N4WS-F1279 drill hole shows several inversions of polarity (five) along the stratigraphy indicating that our sampling likely averages out the secular variation of the geomagnetic field. As we mentioned before, at the bottom part of the N4WS-F1279 core (ca. 56 m), the inclination's plot shows a change in its values, showing values $>30^\circ$ (Fig. 9). For this reason, we divide the results into two groups, Carajás 1 (steep inclination) and Carajás 2 (low inclination), and calculate the mean paleomagnetic pole for each (C1 and C2, respectively) (Fig. 8).

For the C2 group, twenty of the 28 samples show SE direction and eight samples show an antipodal NW direction, both showing low inclination values, so that a reversal test was performed between these clusters. Even though the polarity of most Precambrian paleomagnetic data is completely unconstrained, we assigned polarity as positive and negative by ChRM direction. A primary approach is graphic, showing that the mean positive (SE) and negative polarity (NW) directions are statistically undistinguishable when corrected to the paleohorizontal (Fig. 7). Due to the low inclinations, we preferred a bootstrap reversal test (Koymans et al., 2016) to calculate the mean directions for the two distributions: declination (D_m) = 306.5° , inclination (I_m) = -6.8° ($N = 8$, $k = 10.2$) for the NW direction, and $D_m = 137.9^\circ$, $I_m = 7.1^\circ$ ($N = 20$, $k = 12.6$) for the SE direction. The angular difference between NW and the SE mean directions is $\gamma = 7.6^\circ$ and the critical angle between the means is $\gamma_{cr} = 18.8^\circ$. The test is positive with classification C (McFadden and McElhinny, 1990). These cores were drilled near perpendicular to the bedding at each drilling site. Therefore, no bedding correction was applied to the paleomagnetic data. But since the bedding on each core is different, a paleomagnetic “fold test” can be attempted (Fig. S3). Unfortunately, as the dips of fold limbs are low, the “fold test” is inconclusive (Tauxe and Watson, 1994). Overall, using both positive and negative site mean directions, 28 sites (C2) in the almost entire section (lava flows 3 to 13; 57 to 728 m) yield a mean site directions cluster around the mean $D_m = 134.3^\circ$, $I_m = 6.8^\circ$ ($N = 28$, cone of 95% confidence $\alpha_{95} = 8.5^\circ$, $k = 11.3$), corresponding to the paleomagnetic pole at 40.5°E , -44.6°S ($A_{95} = 6.5^\circ$, $K = 18.5$) (Fig. 8A).

The second group (C1) consists of only 5 sites from the bottom section of N4WS-F1279 ($<57\ \text{m}$; Fig. 9), which is below the limit to perform a reversal test (McFadden and McElhinny (1990)). The C1 component is characterized by remanent magnetizations southerly directed and with medium downward inclinations. Their site means directions group around $D_m = 156.4^\circ$, $I_m = 54.1^\circ$ ($N = 5$, $\alpha_{95} = 12.5^\circ$, $k = 38.4$) and the C1 paleomagnetic pole is located at 342.4°E , -54.3°S ($A_{95} = 14.8^\circ$, $K = 27.8$) (Table 1; Fig. 8B). It is important to stress that these paleomagnetic poles C1 and C2 were estimated assuming the rotation to PGF. We also calculated the poles considering the rotation to the dipolar field

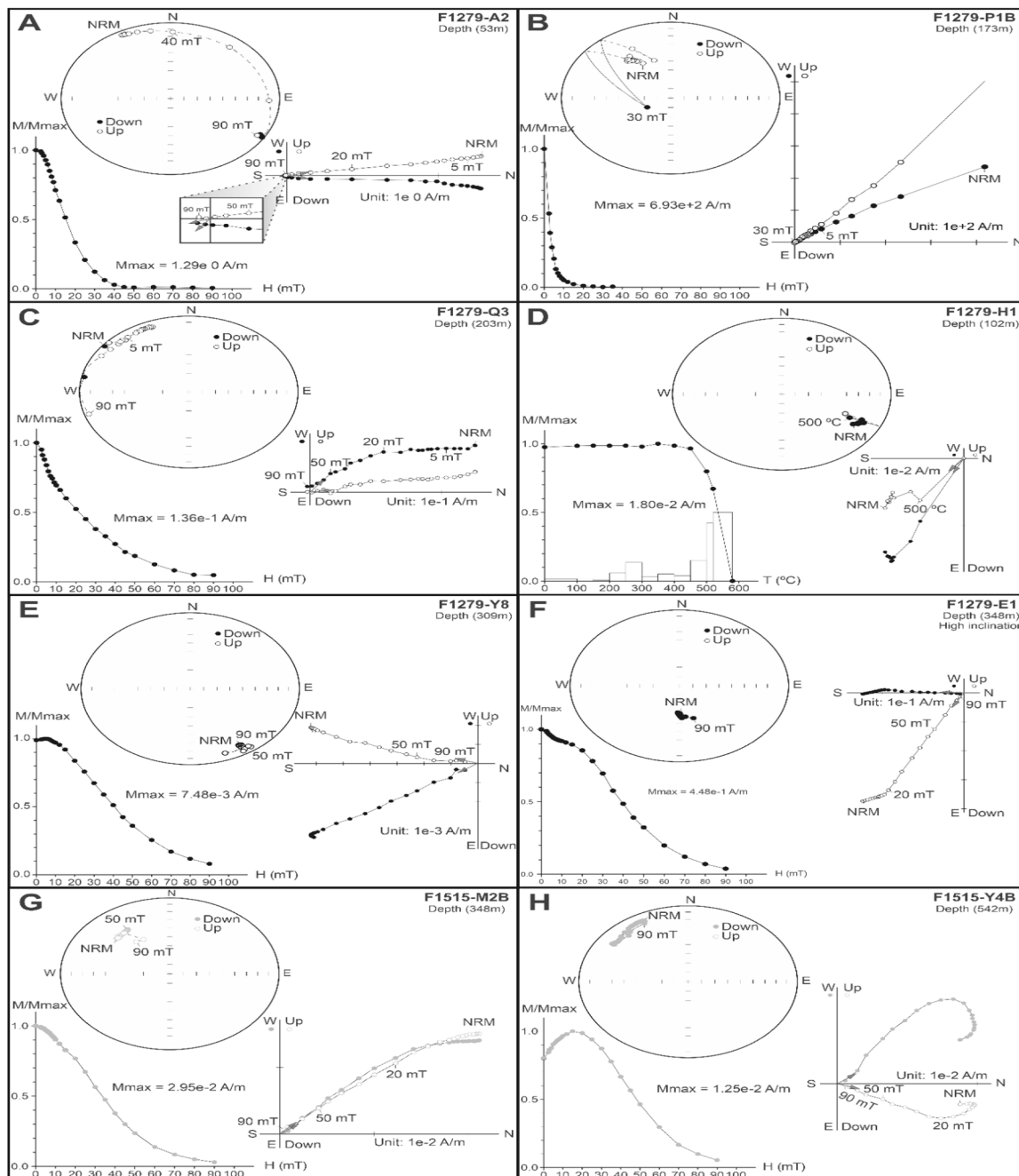


Fig. 7. Examples of AF and thermal demagnetization from the Parauapebas Formation basalts with the viscous component rotated to the present-day field. A-F are examples for basaltic rocks from N4WS - F1279 drill hole (black); G and H are examples from N4WS - F1515 (grey). Demagnetization results are presented with stereographic projections, orthogonal projections and normalized magnetization intensity curves (M/Max versus alternating field H or thermal T).

(Table 1), which imply in rotating the magnetic directions of 18.5° (the local declination) around a vertical axis (see Fig. 8 for the position of PGF and PDF in the sampling sites).

5.1. Baked contact test

Secondary magnetization in igneous (volcanic) rocks may result from physicochemical changes that somehow influence the composition and/or structure of magnetic minerals and must leave an imprint in rock-magnetic properties. Despite the difficulty to describe dykes/sills in drill core samples, we attempted to perform a reversed baked contact test between a small ramification of the Parauapebas magmatism and the host Carajás BIFs where the contact was visible. Fig. 10A is a

schematic sketch showing a Parauapebas-associated gabbroic dyke cross-cutting the Carajás BIF sample. Correlation with SHRIMP dating of zircon grains in the same mafic dyke/sill that cuts the Carajás Formation suggests an age of 2745 ± 5 Ma (Martins et al., 2017) for this sub-volcanic rock. The baked host rock sample (Carajás BIF) taken directly from the bottom contact (Fig. 10A) of a 1 m wide transversal mafic dyke shows a ChRM similar to that of the dyke (Fig. 10B; Table 1). The gabbroic dyke shows mean site directions of $D_m = 140.7^\circ$, $I_m = 39.5^\circ$, $\alpha_{95} = 10.3^\circ$ (Fig. 10B; Table 1). At the contact (<5 cm), the Carajás BIF samples show a similar direction ($D_m = 151.5^\circ$, $I_m = 39.4^\circ$, $\alpha_{95} = 21.9^\circ$) (Fig. 10B; Table 1). Samples collected far away from the contact (>100 m downwards) have a distinct mean direction with $D_m = 301.0^\circ$, $I_m = -31.8^\circ$, $\alpha_{95} = 4.3^\circ$ (Fig. 10B; Table 1). But note that this direction is

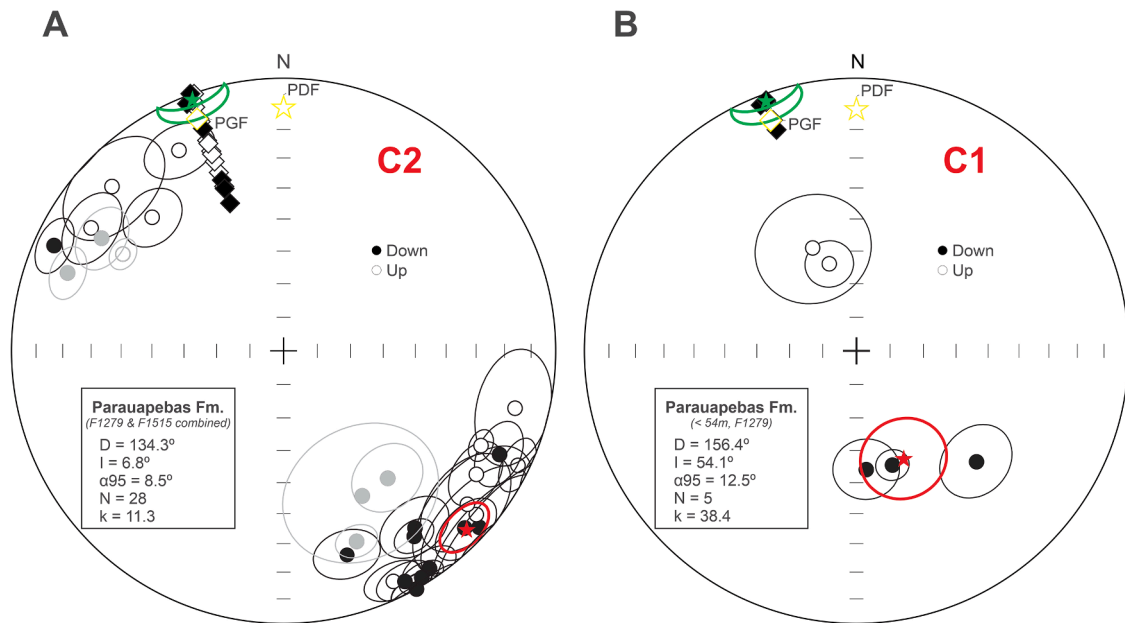


Fig. 8. Stereoplots showing paleomagnetic data per site for the Parauapebas Formation, Carajás Basin. Site mean characteristic remanence directions with circles of 95% confidence for 28 sites from C2 (A) and 5 sites from C1 (B). All directions were rotated in a way that the respective viscous component, represented by diamonds, is aligned with the present-day field. The grand mean of all VRMs is indicated by a green star and its circle of 95% confidence. Each site mean is represented by black symbols for N4WS - F1279 core and grey symbols for N4WS - F1515 core. Red stars in each stereogram represent the grand mean of the characteristic remanence. PDF – Present Dipolar Field; PGF – Present Geomagnetic Field. PDF and PGF are -18.5° apart.

antipodal within error to the direction obtained in the BIF and in the dyke. Therefore, we consider that this baked contact test may suggest the BIF samples near the contact were baked during the intrusion of the dyke at ~ 2745 Ma, however it is nonetheless inconclusive given the record of polarity change throughout the succession. Unfortunately, no paleomagnetic study was performed in the BIF section to provide its full directional record. Additional support for the absence of wholesale remagnetization is the dissimilarity between the ChRM direction obtained here and published younger paleomagnetic directions from the same region, including the Uatamã, Tucumã, and Rio Maria dykes, for which positive baked contact tests were obtained (cf. Antonio et al., 2017, 2021 and references therein). Also, the positive reversal test is consistent with a primary origin for the Parauapebas Formation magnetization. Such features suggest that the magnetization recorded by the lava flows and the dyke reported here was acquired at the time of their cooling and therefore are useful for providing paleogeographic constraints to the Carajás Archean block.

6. Rock magnetism

Identifying magnetic carriers provides crucial information about the magnetization, timing and the geological processes involved during the magnetization of the rock. We applied several rock magnetic analyses to the Neoproterozoic basalts from Parauapebas Formation, including thermomagnetic curves (bulk susceptibility k versus temperature T), hysteresis measurements and isothermal remanent magnetization. Because the rock magnetic characteristics of the studied volcanic rocks were very similar across the cores sampled, we describe their magnetic mineralogy collectively.

6.1. Thermal susceptibility

Thermomagnetic curve (low-field susceptibility versus temperature) is a very useful tool to identify the minerals that carry the magnetic remanence (Hrouda, 1994), as it gives precise information about the Curie Temperature of ferromagnetic materials, characteristic for each mineral (Dunlop and Özdemir, 1997). Thus, high temperature curves

were performed in representative samples. High-temperature thermomagnetic curve in the sample F1279-P shows Curie temperature around 575°C (Fig. 11A), typical of thermally stable magnetite grains (Dunlop and Özdemir, 1997). In all irreversible curves (Fig. 11) susceptibility increases during the cooling phase, indicating that probably magnetite is being formed during heating, producing a new magnetic phase. The sample F1279-P also suggests the development of hematite (Fig. 11A). This behavior was also observed during the thermal demagnetizations. Sample F1279-X shows a curve with irreversible behavior characterized by different trajectories during heating and cooling and small fall between 500 and 600°C indicating the presence of magnetite in small quantity (Fig. 11B).

6.2. Hysteresis and isothermal remanent magnetization curves

Hysteresis loops of the Parauapebas samples are consistent with PSD magnetite characterized by narrow-waisted hysteresis curves (Fig. 12A-C). IRM curves were acquired for 15 specimens and three representative examples are illustrated in Fig. 12D-F. The presence of magnetite in the Parauapebas lava flows is confirmed by IRM curves, which reach saturation at fields up to 0.2 T (Fig. 12D-F), with a negligible contribution of hard-coercivity minerals. Based on thermomagnetic curves, IRM acquisition curves and demagnetization diagrams (Fig. 7), we interpret that the remanence is carried mostly by Ti-poor magnetite. Furthermore, the petrographic observations also support magnetite as the predominant magnetic carrier in these rocks (see Section 4).

The Day plot (Day et al., 1977; Dunlop, 2002) is a powerful tool to visualize the domain state of magnetic minerals, especially magnetite. The Day plot values can be found in the Supplementary Material (Table S1). All studied samples fall into pseudo-single domain (PSD) range or along a trend parallel to the theoretical SD/MD mixing curves of Dunlop (2002) (Fig. 13). According to the Day's diagram, the studied samples contain about 10–40% of SD grains, except for sites F1279-J, F1279-ZB, F1279-ZD and F1279-ZE, which have less ($\sim 10\%$) SD grain contribution (Fig. 13). This behavior is consistent with the good magnetic stability obtained during AF and thermal treatment. For the studied basaltic flows, the PSD magnetite is formed during the magmatic

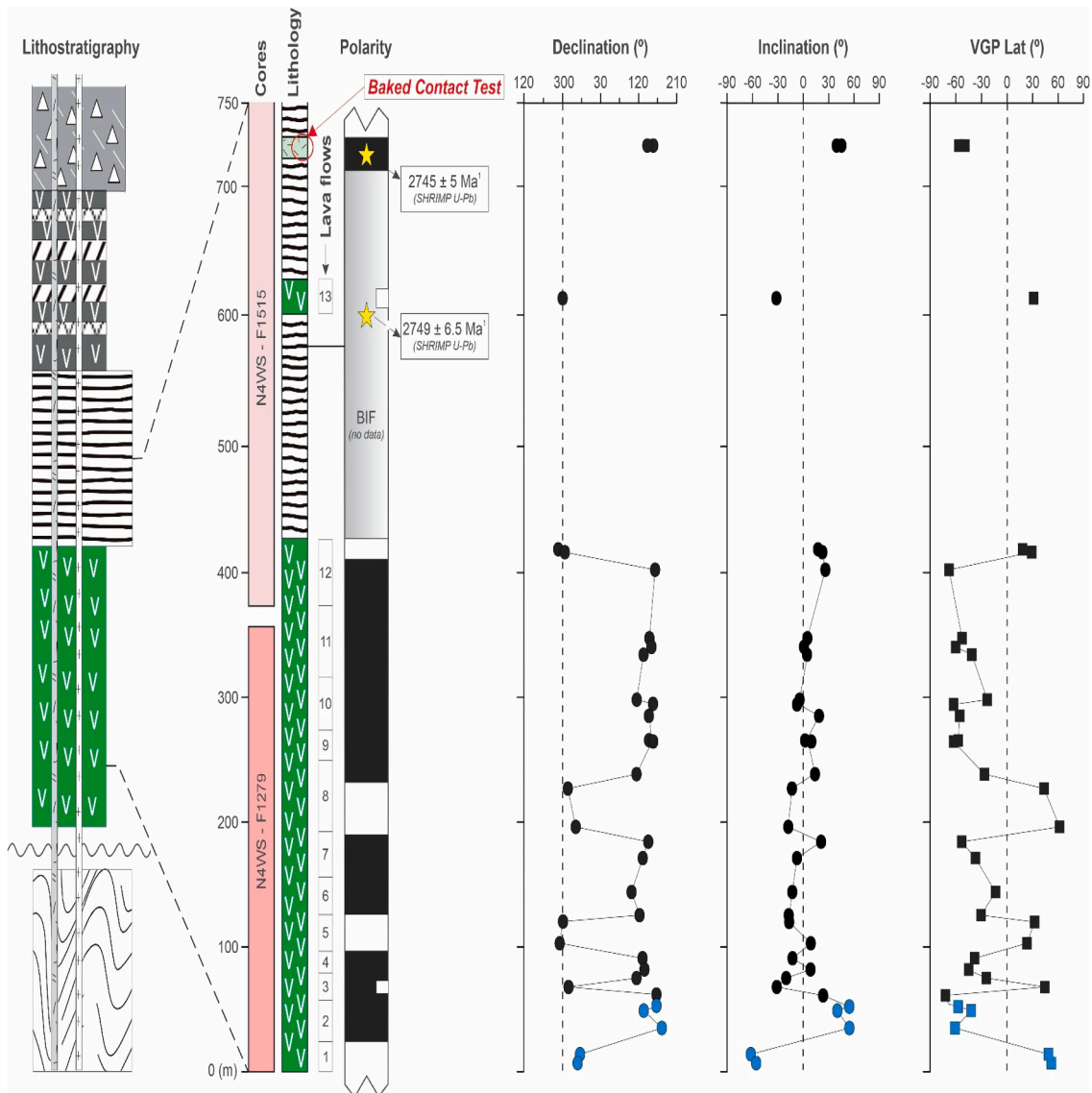


Fig. 9. Magnetostratigraphy from the Parauapebas Formation. Lithostratigraphy, lithology, paleomagnetic sites, ChRM directions, and VGP latitudes per sample for components C1 (sky blue) and C2 (black). The magnetostratigraphy shows several reversals across the stratigraphy and a major shift in paleolatitude between the flows 2 to 3 boundary (~55 m). Positive (SE direction) and negative (NW direction) are indicated, respectively, as black and white zones in the magnetostratigraphic scheme. 1 = Age correlated from Martins et al. (2017). Lithostratigraphy's legend is the same as in Fig. 3.

stage, and no evidence of secondary magnetite was observed.

7. Discussion

7.1. Reliability of paleomagnetic poles

The C2 group is defined using two different drill cores (N4WS-F1279 and N4WS-F1515) as two different locations. The similarity between the two cores strengthens the use of this component as the characteristic remanence of Parauapebas Formation lava flows. It also provides some support for the use of the viscous remanent magnetization to rotate both cores to the true North. We acknowledge that a rotation to the present dipolar field (PDF) is equally valid. In Table 1 both possibilities are presented, with mean directions and paleopoles calculated for the rotations to the present-day geomagnetic field and the dipolar field. Note that the angular difference between PGF and PDF in the region is 18.5°. This choice does not affect the reversals record, or the reported paleolatitudes, but corresponds to a change in the orientation of the Carajás block in the paleogeographic reconstruction. Since most of our following

discussion is based on the paleolatitude of the block, we think this issue does not compromise the final interpretation.

The Parauapebas Formation C2 pole (-44.6°S, 40.5°E, $N = 28$, $A_{95} = 6.5^\circ$) satisfies 4 ($Q = 4$) out of the 6 quality criteria proposed by Meert et al. (2020), if we discard the seventh criterion as suggested in the Paleomag database for Precambrian rocks (Pivarunas et al., 2018). (1) The age is well-defined at 2749 ± 6.5 Ma by correlation with the N4WS-F1338 and the N4WS-F1515 cores which are on the same sequence (Martins et al., 2017). (2) Stable southeastern, low downward/upward inclination (C2 component group) were determined for 171 specimens from 20 out of 28 analyzed sites of the Parauapebas volcanic rocks, and has adequate Fisher's statistical parameters ($A_{95} = 8.5^\circ$, $K = 11.3$) (Table 1). Remanence vectors were well-isolated using stepwise AF treatments, and thermal demagnetizations. They were calculated by the principal component analysis (Kirschvink, 1980) through the visualization of magnetic directions plotted in the Zijderveld diagrams and stereographic projections; (3) The dominant magnetic phase in Parauapebas samples is magnetite, which is supported by the Curie temperature (580–590 °C) determined in the thermomagnetic susceptibility

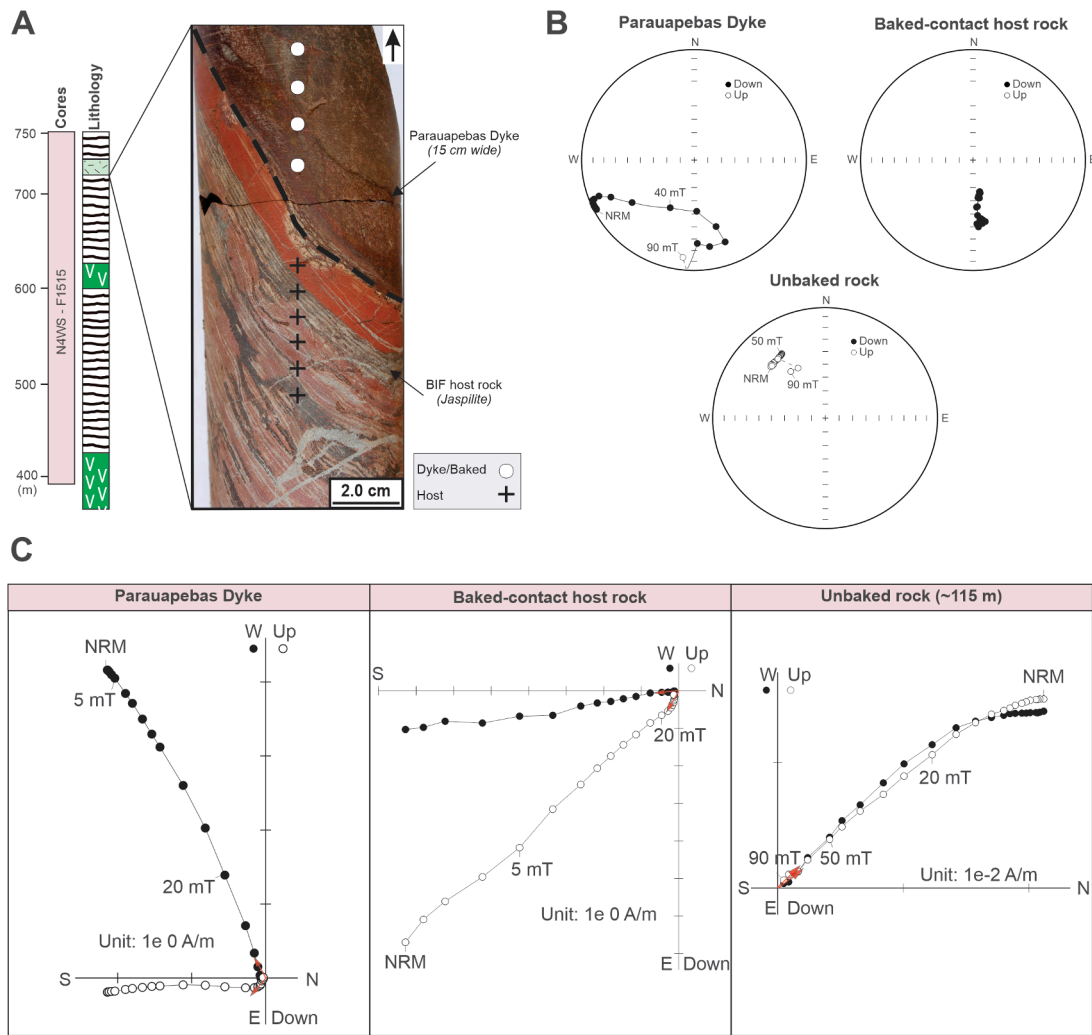


Fig. 10. Parauapebas formation baked contact profile test at location F1515-E (~728 m): A) Location and sampling profile at samples used at baked contact test; B) Stereonet projections showing characteristic behavior of natural remanence to AF demagnetization for three representative samples, near dyke contact (samples F1515-E4Ba and F1515-E5) and unbaked rock sample at ~115 m from the contact (F1515-M2); C) Orthogonal projections (Zijderveld plot) for these representative samples.

experiments (Fig. 11) and by rock magnetic experiments (Figs. 12, 13). (5) No significant metamorphism or deformation is observed in the Parauapebas lava flows and neither in the banded iron formation (upper sequence) in the area (see Martins et al., 2017 for details). (6) Both polarities were observed in the studied samples (Table 1), which implies the secular variation was averaged out. The inconclusive baked contact test and fold tests does not allow to satisfy these criteria. Further studies will have to sample these formations on different flanks of more inclined folds and attempt a more thorough sampling of the host BIFs for the contact test. Furthermore, the pole obtained for component C2 does not match younger paleomagnetic poles for the Amazonian Craton (cf. Antonio et al., 2017, 2021 and references therein), ruling out pervasive remagnetization.

The reliability of the results is also indicated by the well-preserved primary mineral assemblages and igneous textures from the samples (see section 4), in which the secondary alteration observed (mainly chloritization) is attributed to seafloor hydrothermal activity (Martins et al., 2017; Figueiredo e Silva et al., 2020). It implies that these basaltic lava flows were likely not have been heated beyond the blocking temperature of magnetite (~450–550 °C) after their emplacement.

Although more scattered, the C1 directions isolated in the investigated rocks (Fig. 8B) yielded a paleomagnetic pole (-54.3°S, 342.4°E, $A_{95} = 14.8^\circ$) different to the C2 pole. This paleomagnetic pole was

calculated for 2 basaltic flows located at bottom part of Parauapebas Formation (<57 m in stratigraphic height). No age is presently available for these lava flows, or field tests to constrain the age of the C1 paleomagnetic pole.

7.2. Age and correlation of magmatic events

Several lines of evidence are often used to reconstruct the Precambrian paleogeography, including paleomagnetism (Evans, 2013), age of orogens and metamorphic style, distribution of passive margins surrounding central blocks, geological piercing points, detrital zircon provenance and more (Mitchell et al., 2021 and references therein). Among these, two are commonly employed: magmatic barcode matching and paleomagnetism. Bleeker and Ernst (2006) introduced the concept of a magmatic ‘barcode’ record of mafic magmatism through time for specific cratonic blocks which can be easily visualized. Magmatic barcodes provide a convenient graphical representation of the magmatic events within cratons. Each mafic magmatic event from a mafic dyke swarm, sill province, layered intrusion or indeed a continental flood basalt province is defined by a temporal line in the barcode. Similar magmatic barcodes and paleogeographic positions indicate the cratons were probably part of a common crustal framework, whereas divergent magmatic barcodes and paleogeographic position would

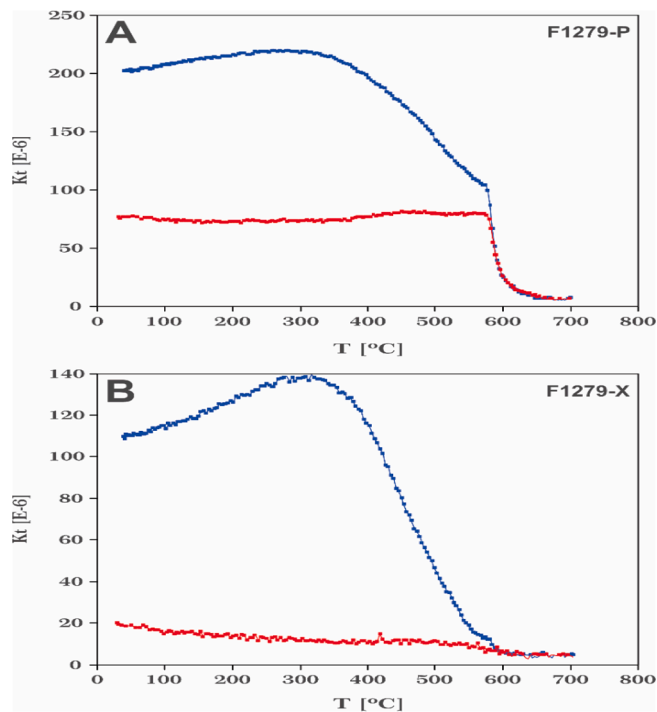


Fig. 11. High temperature thermomagnetic curves from Parauapebas formation. Red and blue curves for heating and cooling, respectively. K_t is bulk susceptibility in International System (SI) units. See main text for details.

indicate the cratons were presumably dispersed during this time interval (e.g., Bleeker, 2004; Bleeker and Ernst, 2006).

Well-exposed and preserved Archean cratons and cratonic fragments typically display numerous episodes of mafic events associated or not with LIPs (Large Igneous Provinces). Although the definition of LIP has become increasingly complex, a LIP is typically defined as a largely mafic magmatic province emplaced over a short time period (e.g., Coffin and Eldholm, 1994; Ernst, 2014). Usually, LIPs are emplaced within 1–5 myr or in multiple short pulses with a maximum duration of a few tens of millions of years and geochemically have intraplate characteristics (Ernst and Youbi, 2017). Due to post-eruption tectonic fragmentation and erosion, the preserved volume of the Parauapebas basalts is less than the minimum required size for a LIP (100,000 km³) (e.g., Ernst, 2014; Ernst et al., 2021). Although many investigators have used areal extent to constrain LIPs sizes (Ernst and Bleeker, 2010; Ernst, 2014), this is difficult to apply to very ancient LIPs such as the Parauapebas where most of the LIP was probably removed by erosion or is not exposed (Condie et al., 2021). However, the available precise geochronological data revealed that the thick volcanic lava sequence was erupted in a relatively short time period of 10–20 myr (Machado et al., 1991; Olszewski et al., 1989; Martins et al., 2017). In addition, the mixture model obtained with zircon grains from volcanoclastic rocks of the Parauapebas magmatism suggests that the zircon population was produced during a short-lived magmatic event (as short as ~ 1 Myr; Rossignol et al., 2021). The thickness of the basalts from Parauapebas Formation (2–3 km; Cabral et al., 2013) is comparable with those of Siberia and Emeishan LIPs (Zhang et al., 2019). As already mentioned, we consider that the tectonic setting of the Parauapebas Formation results from the rifting of older continental crust. Additional support for the classification of the Parauapebas magmatic event as a LIP is the mafic-dominant composition of magmatic rocks (e.g., Martins et al., 2017; Lacasse et al., 2020) and the coeval occurrence of several mafic-ultramafic layered complexes (Ferreira Filho et al., 2007). In summary, if the above-mentioned characteristics are correct, the ca. 2750 Ma igneous activity in Carajás Basin meets at least three

characteristics for a LIP, i.e., short duration, huge thickness and typical rift-like geochemical signatures. Thus, we incorporate the Carajás block in the followed magmatic barcode as a LIP fragment within the Amazonian craton (Rossignol et al., 2021).

Magmatic age barcodes for the southeastern part of the Amazonian craton, Carajás Province, were compared with age barcodes for the Pilbara, Kaapvaal, Superior, Karelia, and Singhbhum cratons (Fig. 14). As we have mentioned before, the ages for the oldest and youngest Parauapebas Formation lava flows vary from 2759 ± 2 Ma (zircon U-Pb age; Machado et al., 1991) to 2749 ± 6.5 (zircon U-Pb age; Martins et al., 2017) (Fig. 3). The age of 2749 ± 6.5 was obtained in the same dataset (C2) used in this study. Ca. 2.75 Ga magmatism coeval with the Parauapebas basalts exist in the stabilized Pilbara (the Fortescue Group), Kaapvaal (the Ventersdorp Group) and Singhbhum (NNE dyke swarm) cratons, and in the non-stabilized Karelia (Panozero) and Superior (Wabigoon tholeiitic dykes) cratons (Fig. 14). Moreover, Pilbara, Kaapvaal and Carajás show similarities between their magmatism in terms of bimodal affinity. The next magmatic age barcode (not shown) match for the Amazonian craton is at ca. 1.89–1.85 Ga (Uatumā event) with other widespread throughout world cratonic areas (e.g., Laurentia, Zimbabwe, Kalahari, Baltica, São Francisco).

In addition to the age of magmatic events, we can also perform these correlations based on the age of the rifting event in the Carajás Basin at ~2.7 Ga, which broadly coincides in time with the break-up of one of the first documented supercontinent (Pesonen et al., 2003; Reddy and Evans, 2009; Eriksson and Condie, 2014; Rossignol et al., 2020; Fig. 14). For instance, the onset of rifting in the Pilbara and Kaapvaal cratons occurred during the course of the Neoproterozoic, at ~ 2.7 Ga (Blake, 1993; Olsson et al., 2010). Furthermore, Rossignol et al. (2020) also illustrated that the Neoproterozoic to Paleoproterozoic tectonic setting of the eastern Amazonian Craton compares with those documented in other major cratons across the world.

Therefore, based on matching ca. 2.75 Ga magmatic barcode and also the similar cratonization ages, it is possible to suggest that Carajás block, Kaapvaal, Pilbara, Singhbhum cratons could have been neighbors in the late Archean. We therefore propose that these blocks were probably part of the same supercraton at this time. The matching 2.75 Ga magmatism also allow us to infer the proximity of Superior and Karelia cratons to this supercraton. As the location of the Carajás block during the Neoproterozoic could be constrained by our new paleomagnetic data, this hypothesis will be discussed further.

7.3. Magnetostratigraphy

The ChRM directions and VGP latitudes of the individual site means for the Parauapebas Formation are plotted from oldest to youngest in Fig. 7. Two particular components of this scheme may prove useful in assisting stratigraphic correlations within the Parauapebas Formation basaltic flows across the Carajás Basin: (i) positive (SE) and negative (NW) directions across the stratigraphy and (ii) a major shift in paleolatitude across the flow 2 to 3 boundary (~55 m; Fig. 9; Fig. 15). Considering that our azimuthal orientation based on the viscous magnetization is correct, at least six magnetic reversal events are identified in the composite lava flow sequence from the two cores (Fig. 9; Fig. 15). A multi-polarity record and fast paleolatitudinal movements were also obtained for 2775–2715 Ma rocks from the East Pilbara Basin (Strik et al., 2003). Given the indetermination of polarities and the uncertainties in ages on both successions, we cannot propose a direct correlation between these two units, but their configuration raises the possibility that these geomagnetic reversals represent some of the oldest known geomagnetic field reversals, as already proposed by Strik et al. (2003).

The reconstructed paleolatitudes from the Carajás Basin revealed a major change in the paleolatitude position (C1 = 34.6 ± 12.5 to C2 = 3.4 ± 8.5°; Fig. 15) across the flow 2 to 3 boundary (~55 m, C1 to C2). No geochemical or petrographic change along the basaltic succession is

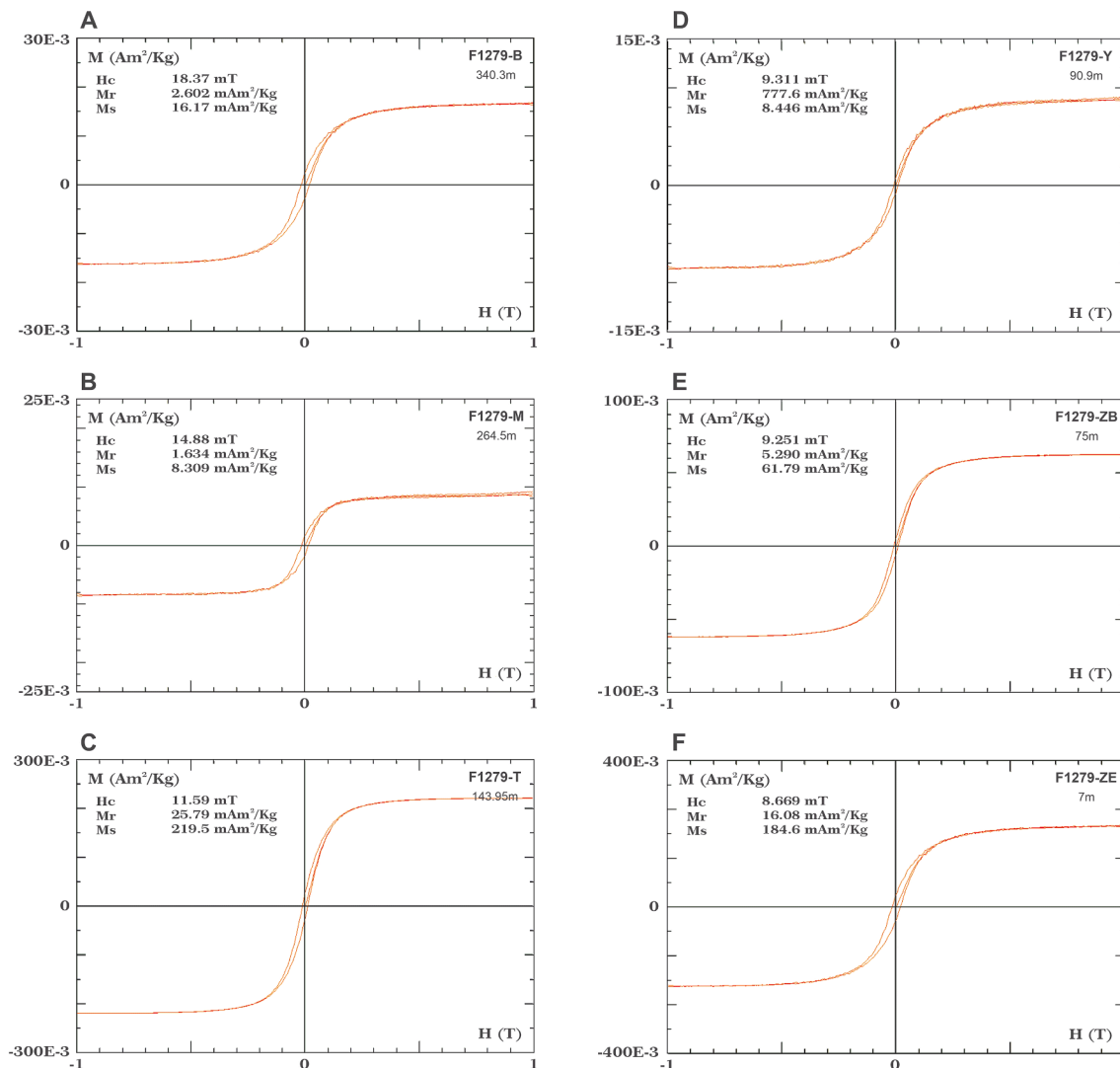


Fig. 12. Representative hysteresis loops (A-C) and isothermal remanent acquisition (IRM) curves (D-F) of the Parauapebas Formation after paramagnetic slope correction.

observed coincident with the paleolatitudinal shift found (cf. Martins et al., 2017). This difference in paleolatitude (average of 31.2°) is significant and is not related to changes in core dip or to changes in the attitude of the volcanic beds, which remains constant throughout the drilled succession. It may result from a local field excursion, a fast latitudinal movement of the Carajás block between flow 2 and flow 3, or from an age gap along the volcanic sequence. Since the direction was recorded coherently in two distinct lava flows, we exclude the possibility that all of them record an anomalous, short field excursion. However, the lack of a precise radiometric dating for the basal flows (C1 sites) does not allow us to define whether this variation reflects an age gap or a fast latitudinal movement. With this in mind, and considering the weakness of the C1 pole, we conclude that the C1 pole cannot be used as an appropriate reference pole for constraining the Carajás paleogeography. Furthermore, the mean paleolatitude position of the remaining flows (C2 sites) implies that no significant latitudinal movement occurred within the error of our paleomagnetic results during extrusion of the volcanic succession.

7.4. Implications for Archean supercratons

The hypothetical supercontinent formed by the end of the Neoproterozoic has been given the name Kenorland. The name was suggested

for the first time by Williams et al. (1991) after the 2.7 Ga Kenoran orogeny consolidating the Superior craton in North America. The alternative to a united Kenorland supercontinent is a paleogeographic model of distinct, freely drifting, continent-sized supercratons, including Superia, Sclavia and Vaalbara – each containing several modern cratons with characteristic ages of amalgamation, ca. 2.7, 2.6 and 2.9 Ga, respectively (Bleeker, 2003; Evans et al., 2016).

One of the earliest known potential Archean crustal configurations is that of Vaalbara (e.g., Cheney, 1996; de Kock et al., 2009), which incorporates ancient crust in southern Africa (Kaalvaal) and Western Australia (Pilbara). The connection between the Pilbara and Kaalvaal cratons begins with a comparison between the geology and geochronology of both cratons, and the parallel development of the Neoproterozoic-Paleoproterozoic stratigraphy that is the core of the Vaalbara hypothesis. In particular, good indicators are the Paleoproterozoic iron formations (Trendall, 1968), but there are also broader links between the 3.5 Ga and 1.8 Ga volcano-sedimentary basins and mineral deposits (e.g., Button, 1976; Cheney, 1996). Since these early contributions, new paleomagnetic data have become available that can both support and discredit the concept of Vaalbara. Initial data did not support the concept of Vaalbara (Wingate, 1998). The author used paleopoles from both cratons to conclude that by ~ 2.78 Ga the two cratons were not contiguous, being latitudinally separated. However, further study of the

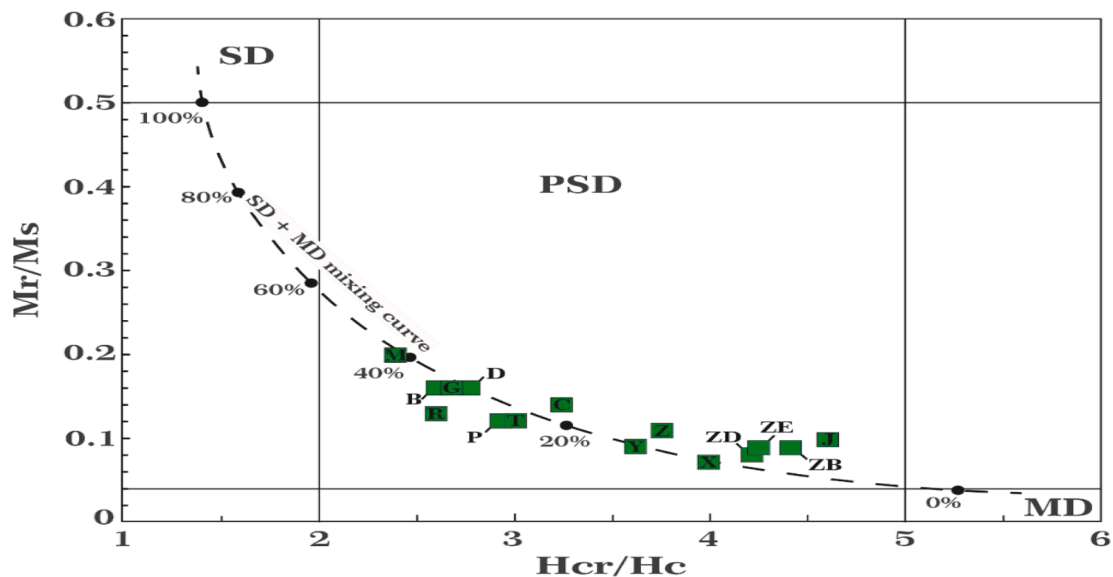


Fig. 13. Day diagram modified by Dunlop (2002), indicating the state of domain of magnetites. Samples from Parauapebas Formation correspond to the pseudo-single domain (PSD) field. Dashed line represents the theoretical mixing curve for MD grains at different percentages (black dots) with SD magnetite (Dunlop, 2002). Magnetic parameters used to construct this diagram are given in Supplementary Table 1.

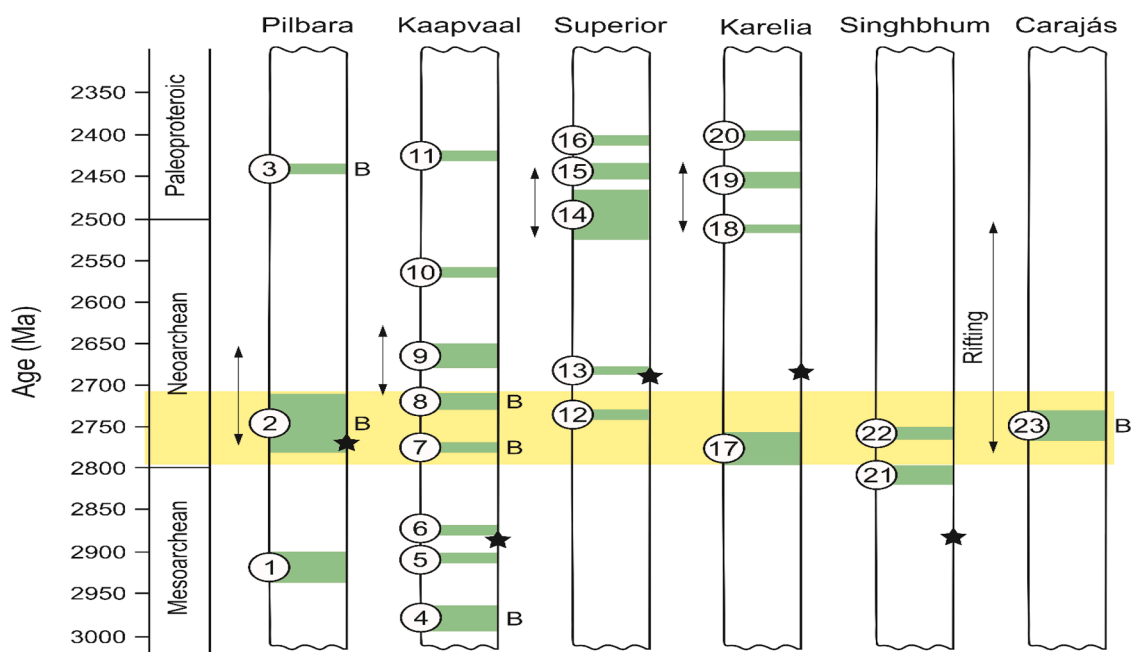


Fig. 14. Magmatic barcode for some of the Archean cratons, with each individual magmatic event denoted. These include the following events (dyke swarms, sill provinces, and other components of LIPs): 1 - Munni Munni; 2 - Fortescue; 3 - Woongarra; 4 - Nsuze; 5 - Crown; 6 - Hlagothi; 7 - Derdepoort; 8 - Ventersdorp; 9 - Rykoppies-White Mfolozi; 10 - Mvunyana; 11 - Ongeluk; 12 - Wabigoon; 13 - Otto; 14 - Ptarmigan-Mistassini; 15 - Matachewan R; 16 - Matachewan N; 17 - Panozero; 18 - Shalskiy; 19 - Burakovka; 20 - Taivalkoski; 21 - Malaigiri; 22 - Singhbhum NNE dykes; 23 - Parauapebas. The width of individual bars corresponds to the 2σ error in radiometric ages and 'B' denotes bimodal magmatism. Black stars denote the end of cratonization for each craton (Bleeker, 2003; Halla, et al., 2017). Data mostly from Ernst and Buchan, 2001. The arrow indicates the range of rifting ages. Pilbara Craton after Blake, (1993), Kaapvaal Craton after Olsson et al. (2010), Karelian-Kola Craton after Amelin et al. (1995) and Superior Craton after Ernst and Bleeker (2010).

Pilbara region (Strik et al., 2003) modified its paleolatitude, leading to the conclusion that the Vaalbara hypothesis cannot be rejected. For later times, de Kock et al. (2009) reported new 2.70 Ga data from Kaapvaal and have attempted a reconstruction using pairs of poles from the Pilbara and Kaapvaal cratons. Using the same procedure with somewhat older paleopoles (2.78 Ga), Denyszyn et al. (2013) updated and supported the reconstruction reported by de Kock et al. (2009). The pendulum swings back again by the new data for the Black Range Suite

(Evans et al., 2017), from which the authors question the correlation at 2.78 Ga. The existence of a unified Vaalbara supercraton is also discredited by Evans and Muxworthy (2019) that presented an updated analysis which showed that the existence of a single supercraton between ~2.9 and ~2.7 Ga is inconsistent with the available palaeomagnetic data. Therefore, a robust Vaalbara reconstruction remains elusive.

Recently, Kumar et al. (2017) showed the broad geochronological and paleomagnetic similarity between the Kaapvaal and Singhbhum

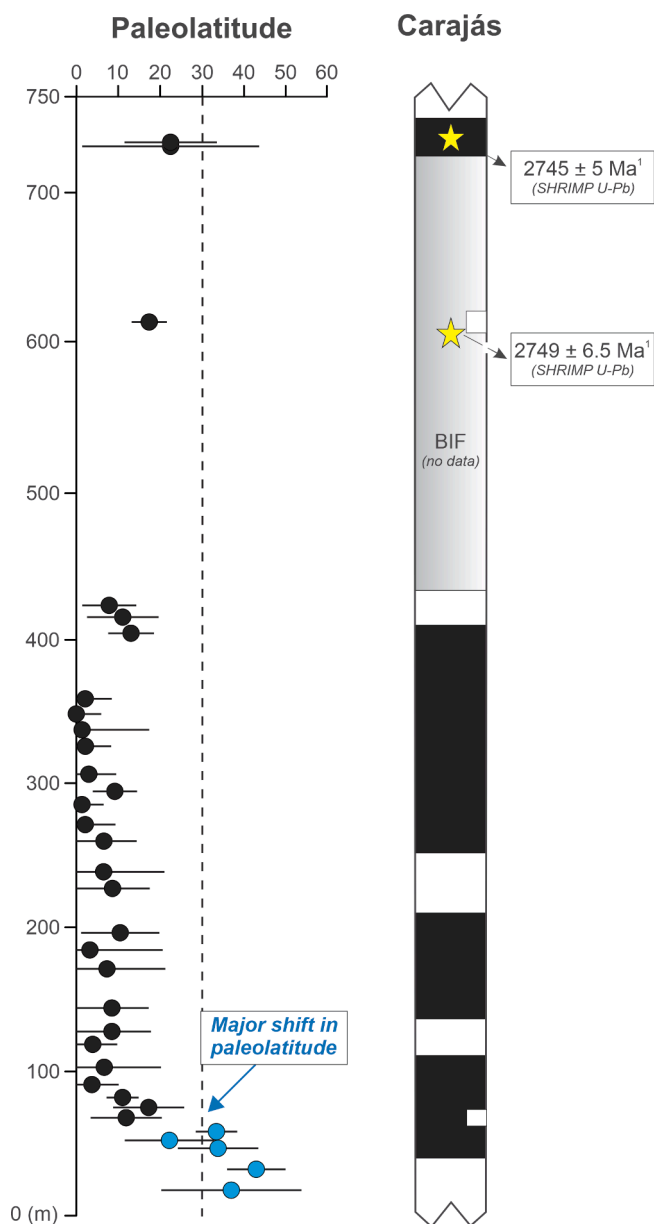


Fig. 15. Magnetic stratigraphy of Carajás Basin (Parauapebas Fm.). A major change in paleolatitude position (average of 31.2°) between sites 28 and 29 (C1 to C2) is noteworthy. Positive (SE direction) and negative (NW direction) are indicated as black and white zones in the magnetostratigraphic scheme, respectively. C1 = sky blue and C2 = black.

Craton in India at 2.81–2.76 Ga. In their analysis, Kumar and colleagues suggested that Singhbhum Craton was also likely part of Vaalbara configuration at this time. Later, Gumsley (2017) and Gumsley et al. (2017) proposed that these cratons were not nearest neighbors but were instead parts of a much larger supercraton named Supervaalbara. This supercraton included the Superior, Wyoming, Hearne, Kola + Karelia, Kaapvaal, Pilbara, and perhaps Singhbhum cratons. Furthermore, Salminen et al. (2019) followed these authors and demonstrated that Uauá block, a fragment of São Francisco craton, could have been part of the Supervaalbara supercraton by 2.62 Ga. As an alternative hypothesis, Liu et al. (2021) proposed that the different apparent polar wander (APW) paths of Superia (a supercraton surrounding the Superior Craton), Yilgarn and other cratons are inconsistent with a single Archean supercontinent and supportive of the existence of another supercraton geographically distant from Superia.

Integrating our new paleomagnetic data of component (C2), the magmatic barcodes (see section 7.2) and paleopoles compiled from other Archean cratons (Table 2) that could have been part of the hypothetical supercontinent, we illustrate a plausible Archean position for the Carajás block (Carajás Archean Province) with respect to these cratons during ~ 2750 Ma (Fig. 16). The details of selected high-quality 2780–2720 Ma paleomagnetic poles are shown in Table 2. Because of some similar geological records (e.g., coeval bimodal magmatism), we reconstruct the Carajás block close to the Superior craton. At ~ 2750 Ma, Carajás restores to $3.4 \pm 8.5^\circ$ paleolatitude (Fig. 16B). Singhbhum is reconstructed at high latitudes and could have been proximal to the Vaalbara (Pilbara + Kaapvaal) supercraton during this time (Kumar et al., 2017). The matching of ~ 2750 Ma magmatism and overlapping paleolatitudes also support the proximity with the Karelia craton (Fig. 16). Note that longitude is not constrained in paleogeographic reconstructions based on paleomagnetism but our proposed paleogeography is consistent with geological observations (Fig. 14). A comparison of absolute polarities with other cratonic units could constrain the relative position of some Archean cratons and the Carajás block. However, the near equatorial position of Carajás complicates possible interpretation of the reversal record.

The ca. 2.75 Ga poles of Carajás (C2) and Superior put them at similar paleolatitudes (Fig. 16B), tentatively allowing their proximity. This proposal also relies on geologic means of correlation, using approaches such as comparing magmatic barcodes (Fig. 14). By incorporating regional paleogeographic models (Bleeker, 2003) into the global reconstruction for the studied time, we have led to the proposal of adding Carajás block to the larger Superia supercraton, the ancestral landmass of which the Superior craton is the central and largest fragment (Bleeker, 2003). As currently reconstructed (Gumsley et al., 2017; Liu et al., 2021), the Superia supercraton is estimated to have been about the size of modern-day Antarctica (Mitchell et al., 2021), and, so, is much smaller than any of the three established supercontinents (Columbia, Rodinia, and Pangea).

The initial proposed connection between Carajás block, Kaapvaal, Pilbara, and Singhbhum cratons (known as the Vaalbara supercraton) between ~ 2.75 Ga is inconsistent on paleomagnetic grounds. Overlapping the paleomagnetic poles results in a minimum geographic separation of Carajás and Vaalbara of ~ 4000 km (Fig. 16B), which is suggestive of separate supercontinents at this time, similar to the hypotheses of the existence of at least two independent supercontinents during the late Archean tectonic regime (Liu et al., 2021). The insertion of Carajás in a single supercontinent configuration would only be possible if essentially Superior and Karelia cratons plus all remaining Archean cratons not considered here, due to a lack of constraints, occurred to exactly fill the gap between Carajás and Vaalbara. This configuration leads to a dramatically elongated supercontinent trending N-S.

Therefore, our Neoproterozoic reconstruction based on a modest amount of paleomagnetic data and comparison of magmatic barcodes supports the Carajás block could have been part of the Superia supercraton. Due to the limited amount of Archean-Paleoproterozoic paleomagnetic data for the Amazonian craton, we are currently unable to test the duration of this configuration more precisely.

8. Conclusion

We report the first robust paleomagnetic data for the Carajás Province during the Neoproterozoic (~ 2750 Ma). We used paleomagnetic methods to isolate two characteristic components (C1 and C2) and calculate the mean paleomagnetic pole for each: C1 (~ 2759 Ma; 40.5° E, -44.6° S, $N = 5$, $A_{95} = 6.5^\circ$, $K = 18.5$) and C2 (~ 2749 Ma; 342.4° E, -54.3° S, $N = 28$, $A_{95} = 14.8^\circ$, $K = 27.8$). The restored paleomagnetic directions pass a provisional baked contact test within the ~ 2740 Ma Carajás banded iron formation. These observations, combined with petrography and rock magnetic results, suggest a primary origin for the magnetization. At least six possible magnetic reversal events are

Table 2
Selected high-quality ca. 2780–2720 Ma global paleomagnetic poles.

Code	Rock Unit	Age (Ma)	Age References	Plat (°N)	Plong (°E)	A ₉₅	R	References
CARAJÁS (C)								
C1	Parauapebas Fm. 1	2759 ± 2	Machado et al. (1991)	-54.3	342.4	14.8	3	This study
C2	Parauapebas Fm. 2	2749 ± 6.5	Martins et al. (2017)	-44.6	40.5	6.5	4	This study
KAAPVAAL (K)								
K1	Modipe gabbro	2784 ± 1	Denyszyn et al. (2013)	-47.6	12.4	8.6	5	Denyszyn et al. (2013)
K2	Derdepoort basalt	2782 ± 5	Wingate (1998)	-39.6	4.7	17.5	6	Wingate (1998)
KARELIA (Ka)								
Ka1	Panozero sanukitoids	2765 ± 8	Sergeyev et al. (2007)	-10.2	226.1	4.1	5	Lubnina and Slabunov (2009)
PILBARA (P)								
P1	Mount Roe Basalts	~2770	Van Kranendonk et al. (2006)	-52.4	178.0	7.6	7	Schmidt and Embleton (1985)
P2	Pilbara Package 1	2771 ± 7	Arndt et al. (1991)	-41.0	160.0	3.7	6	Strik et al. (2003)
P3	Pilbara Package 2	2766 ± 2	Blake et al. (2004)	-46.5	152.7	15.2	3	Strik et al. (2003), Blake et al. (2004)
P4	Pilbara Package 4–7	2720–2740	Blake et al. (2004)	-50.4	138.2	12.5	4	Strik et al. (2003), (Blake et al. 2004)
SINGHBHUM (Si)								
Si	NNE Dykes	2762 ± 2	Kumar et al. (2017)	14.0	78.0	11	5	Kumar et al. (2017)
SUPERIOR (Su)								
Su1	Dobie Lake batholith	2747 ± 3	Corfu and Stott (1989)	87.3	307.1	27.8	4	Hale and Lloyd (1990)
Su2	Wabigoon gabbro	2732 ± 1	Morrison et al. (1985)	-10.7	200.2	7.5	4	Dunlop (1983)

Code, corresponds to the code in Fig. 14. Plat, Plong are pole latitude and longitude. A₉₅, 95% confidence circle of the pole. N: number of sites studied. R: Reliability criteria (Meert et al., 2020). For Superior and Karelia cratons, the north poles are used.

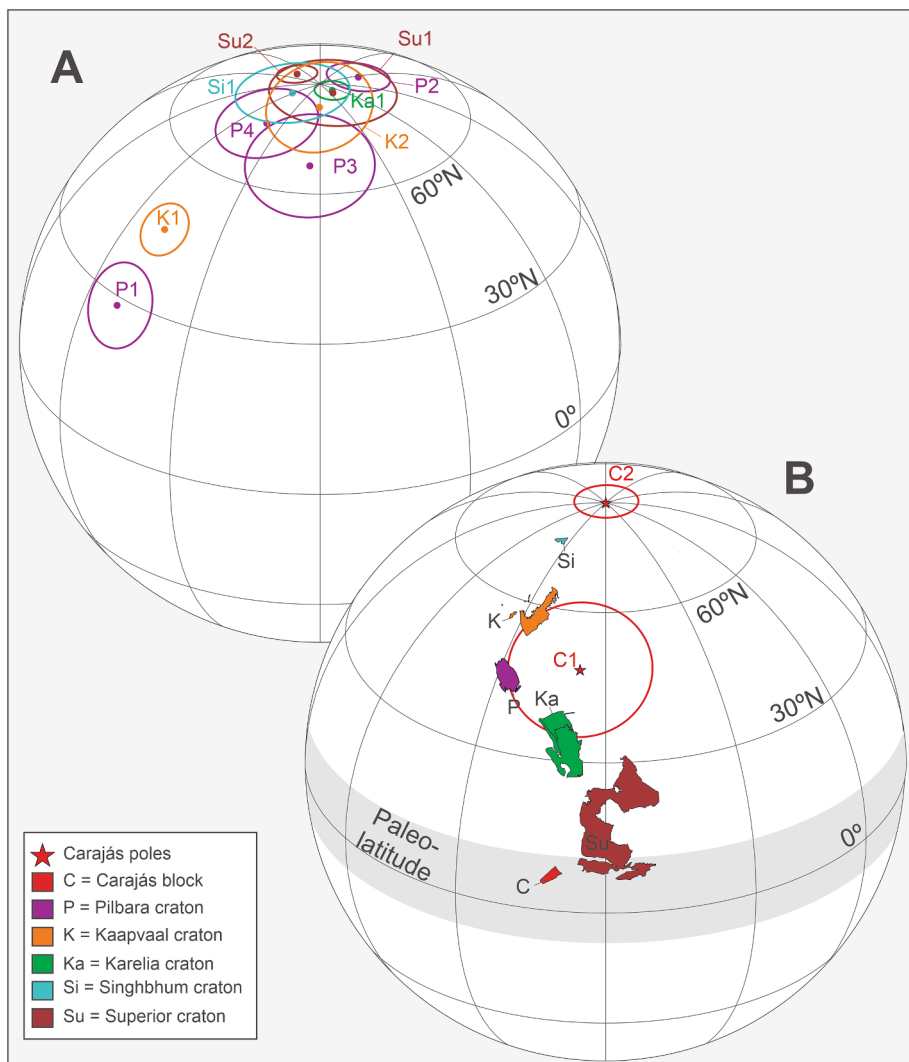


Fig. 16. A plausible paleogeographic reconstruction for the Carajás block with respect to the Pilbara + Kaapvaal (Vaalbara), Karelia, Singhbhum and Superior cratons at ca. 2780–2720 Ma (after de Kock et al., 2009, Kumar et al., 2017; Salminen et al., 2019). (A) Paleomagnetic poles used for the reconstruction and respective acronyms (as in Table 2); (B) paleomagnetic poles for components C1 and C2 and the position of continental blocks. Carajás’s band of allowed paleolatitudinal reconstructions is shown.

identified in the lava flow sequence from the Carajás Basin. A multi-magnetic reversal record was obtained for coeval lava flows from 2775 to 2715 Ma rocks in the East Pilbara Basin reinforcing these findings. Finally, our paleomagnetic investigation integrated with the comparison of geological features reveals that the Carajás block could have been part of the Superia supercraton configuration during the Neoproterozoic (~2750 Ma) in a position close to the paleoequatorial line.

CRedit authorship contribution statement

Pedro L.G. Martins: Conceptualization, Methodology, Investigation, Data curation, Writing – original draft, Visualization. **Catarina L. B. Toledo:** Conceptualization, Investigation, Supervision, Project administration, Writing - review & editing, Funding acquisition. **Adalene M. Silva:** Investigation, Supervision, Project administration, Writing - review & editing, Funding acquisition. **Paul Y.J. Antonio:** Conceptualization, Data curation, Writing - review & editing. **Farid Chemale:** Conceptualization, Resources, Writing - review & editing. **Luciano M. Assis:** Resources, Funding acquisition. **Ricardo I.F. Trindade:** Resources, Supervision, Writing - review & editing.

Declaration of Competing Interest

The authors declare that they have no known competing financial interests or personal relationships that could have appeared to influence the work reported in this paper.

Acknowledgements

The authors wish to extend their special thanks to Vale S.A. mining company for permitting the use of geological data and access to the N4 deposit, as well as providing research funding. Further, we would like to thank the staff at Precambrian Research and editor Wilson Teixeira for all their assistance throughout the publication process. The authors are also grateful to the detailed and constructive review of Michiel de Kock and Augusto Rapalini. This study was financed in part by the Coordenação de Aperfeiçoamento de Pessoal de Nível Superior - Brasil (CAPES) - Finance Code 001. We would like to also thank the Fundação de Apoio à Pesquisa do Distrito Federal (FAPDF) (Nº 00193.00000072/2019-19) for supporting this research. Catarina L.B. Toledo, Adalene M. Silva, Farid Chemale Jr. and Ricardo I.F. Trindade thank the Conselho Nacional de Desenvolvimento Científico e Tecnológico (CNPq) for their respective research grants. The first author Pedro L. G. Martins thanks the CNPq for a PhD scholarship at the Instituto de Geociências (Universidade de Brasília).

Appendix A. Supplementary data

Supplementary data to this article can be found online at <https://doi.org/10.1016/j.precamres.2021.106411>.

References

- de Almeida, F.F.M., Hasui, Y., de Brito Neves, B.B., Fuck, R.A., 1981. Brazilian structural provinces: an introduction. *Earth Sci. Rev.* 17 (1-2), 1–29. [https://doi.org/10.1016/0012-8252\(81\)90003-9](https://doi.org/10.1016/0012-8252(81)90003-9).
- Almeida, J.A.C., Dall'Agnol, R., Oliveira, M.A., Macambira, M.J.B., Pimentel, M.M., Rämö, O.T., Guimarães, F.V., Leite, A.A.S., 2011. Zircon geochronology and geochemistry of the TTG suites of the Rio Maria granite-greenstone terrane: implications for the growth of the Archean crust of Carajás Province. *Brazil. Precambrian Res.* 187, 201–221. <https://doi.org/10.1016/j.precamres.2011.03.004>.
- Almeida, J.A.C., Dall'Agnol, R., Leite, A.A.S., 2013. Geochemistry and zircon geochronology of the Archean granite suites of the Rio Maria granite-greenstone terrane, Carajás Province. *Brazil. J. S. Am. Earth Sci.* 42, 103–126. <https://doi.org/10.1016/j.jsames.2012.10.008>.
- Amelin, Y.V., Heaman, L.M., Semenov, V.S., 1995. U-Pb geochronology of layered mafic intrusions in the eastern Baltic Shield: implications for the timing and duration of Paleoproterozoic continental rifting. *Precambrian Res.* 75 (1-2), 31–46. [https://doi.org/10.1016/0301-9268\(95\)00015-W](https://doi.org/10.1016/0301-9268(95)00015-W).
- Antonio, P.Y.J., D'Agrella-Filho, M.S., Trindade, R.I.F., Nédélec, A., de Oliveira, D.C., da Silva, F.F., Roverato, M., Lana, C., 2017. Turmoil before the boring billion: Paleomagnetism of the 1880–1860Ma Uatamã event in the Amazonian craton. *Gondwana Res.* 49, 106–129. <https://doi.org/10.1016/j.gr.2017.05.006>.
- Antonio, P.Y.J., D'Agrella-Filho, M.S., Trindade, R.I.F., Nédélec, A., Poujol, M., Sanchez, C., Dantas, E.L., Dall'Agnol, R., Teixeira, M.F.B., Proietti, A., Martínez Dopico, C.L., Oliveira, D.C., Silva, F.F., Marangoanha, B., Trindade, R.I.F., 2021. New constraints for paleogeographic reconstructions at ca. 1.88 Ga from geochronology and paleomagnetism of the Carajás dyke swarm (eastern Amazonia). *Precambrian Res.* 353, 106039. <https://doi.org/10.1016/j.precamres.2020.106039>.
- Araújo, R., Nogueira, A., 2019. Serra Sul diamictite of the Carajás Basin (Brazil): a Paleoproterozoic glaciation on the Amazonian craton. *Geology* 47, 1166–1170. <https://doi.org/10.1130/G46923.1>.
- Araújo Filho, Roberto Costa, Nogueira, Afonso C.R., Araújo, Raphael Neto, 2020. New stratigraphic proposal of a Paleoproterozoic siliciclastic succession: implications for the evolution of the Carajás Basin, Amazonian craton. *Brazil. J. S. Am. Earth Sci.* 102, 102665. <https://doi.org/10.1016/j.jsames.2020.102665>.
- Arndt, N.T., Nelson, D.R., Compston, W., Trendall, A.F., Thorne, A.M., 1991. The age of the Fortescue Group, Hamersley Basin, Western Australia, from ion microprobe zircon U-Pb results. *Aust. J. Earth Sci.* 38 (3), 261–281. <https://doi.org/10.1080/08120099108727971>.
- Audunsson, H., Levi, S., 1989. Drilling-induced remanent magnetization in basalt drill cores. *Geophysical Journal International* 98, 613–622. <https://doi.org/10.1111/j.1365-246X.1989.tb02294.x>.
- Blake, Tim S., 1993. Late Archean crustal extension, sedimentary basin formation, flood basalt volcanism and continental rifting: the Nullagine and Mount Jope Supersequences. *Western Australia. Precambrian Res.* 60 (1-4), 185–241. [https://doi.org/10.1016/0301-9268\(93\)90050-C](https://doi.org/10.1016/0301-9268(93)90050-C).
- Blake, T.S., Buick, R., Brown, S.J.A., Barley, M.E., 2004. Geochronology of a Late Archean flood basalt province in the Pilbara Craton, Australia: constraints on basin evolution, volcanic and sedimentary accumulation, and continental drift rates. *Precambrian Res.* 133 (3-4), 143–173. <https://doi.org/10.1016/j.precamres.2004.03.012>.
- Bleeker, W., 2003. The late Archean record: a puzzle in ca. 35 pieces. *Lithos* 71 (2-4), 99–134. <https://doi.org/10.1016/j.lithos.2003.07.003>.
- Bleeker, W., 2004. Taking the pulse of planet Earth: A proposal for a new multi-disciplinary flag-ship project in Canadian solid earth sciences. *Geoscience Canada* 31, 4. <https://journals.lib.unb.ca/index.php/gc/article/view/2776/3260>.
- Bleeker, W., Ernst, R., 2006. Short-lived mantle generated magmatic events and their dyke swarms: the key unlocking Earth's paleogeographic record back to 2.6 Ga. In: Hanski, E., Mertanen, S., Rämö, T., Vuollo, J. (Eds.), *Dyke Swarms - Time Markers of Crustal Evolution*. Taylor & Francis, London, pp. 3–26.
- Buchan, K.L., Mertanen, S., Park, R.G., Pesonen, L.J., Elming, S.-Å., Abrahamsen, N., Bylund, G., 2000. Comparing the drift of Laurentia and Baltica in the Proterozoic: the importance of key palaeomagnetic poles. *Tectonophysics* 319 (3), 167–198. [https://doi.org/10.1016/S0040-1951\(00\)00032-9](https://doi.org/10.1016/S0040-1951(00)00032-9).
- Button, A., 1976. Transvaal and Hamersley Basins – review of basin development and mineral deposits. *Miner. Sci. Eng.* 8, 262–290.
- Cabral, A.R., Creaser, R.A., Nägler, T., Lehmann, B., Voegelin, A.R., Belyatsky, B., Paşava, J., Seabra Gomes, A.A., Galbiatti, H., Böttcher, M.E., Escher, P., 2013. Trace-element and multi-isotope geochemistry of Late-Archean black shales in the Carajás iron-ore district. *Brazil. Chem. Geol.* 362, 91–104. <https://doi.org/10.1016/j.chemgeo.2013.08.041>.
- Cawood, Peter A., Hawkesworth, Chris J., Pisarevsky, Sergei A., Dhuime, Bruno, Capitano, Fabio A., Nebel, Oliver, 2018. Geological archive of the onset of plate tectonics: *Philosophical Transactions of the Royal Society: Mathematical, Physical, and Engineering Sciences* 376 (2132), 20170405. <https://doi.org/10.1098/rsta.2017.0405>.
- Cheney, E.S., 1996. Sequence stratigraphy and plate tectonic significance of the Transvaal succession of southern Africa and its equivalent in Western Australia. *Precambrian Res.* 79 (1-2), 3–24. [https://doi.org/10.1016/0301-9268\(95\)00085-2](https://doi.org/10.1016/0301-9268(95)00085-2).
- Condie, K.C., Pisarevsky, S.A., Puetz, S.J., 2021. LIPs, orogens and supercontinents: The ongoing saga. *Gondwana Res.* 96, 105–121. <https://doi.org/10.1016/j.gr.2021.05.002>.
- Coffin, Millard F., Eldholm, Olav, 1994. Large igneous provinces: Crustal structure, dimensions, and external consequences. *Reviews of Geophysics* 32 (1), 1. <https://doi.org/10.1029/93RG02508>.
- Cohen, K.M., Finney, S.C., Gibbard, P.L., Fan, J.-X., 2013. The ICS international chronostratigraphic chart (updated). *Episodes* 36 (3), 199–204.
- Cogné, J.P., 2003. PaleoMac: A Macintosh™ application for treating paleomagnetic data and making plate reconstructions. *Geochem. Geophys. Geosyst.* 4, 1007. <https://doi.org/10.1029/2001GC000227>.
- Cordani, U.G., Teixeira, W., 2007. Proterozoic accretionary belts in the Amazonian Craton. *Geological Society of America Memoirs* 200, 297–320. [https://doi.org/10.1130/2007.1200\(14\)](https://doi.org/10.1130/2007.1200(14)).
- Corfu, F., Stott, G.M., 1989. U-Pb geochronology of the central Uchi subprovince, NW Ontario. *Geol. Assoc. Can. Annu. Mtg., Program with Abstracts* 14, A55. <https://doi.org/10.1139/e93-100>.
- D'Agrella-Filho, M.S., Bispo-Santos, F., Trindade, R.I.F., Antonio, P.Y.J., 2016. Paleomagnetism of the Amazonia Craton and its role in paleocontinents. *Brazilian Journal of Geology* 46, 275–299. <https://doi.org/10.1590/2317-4889201620160055>.
- Dall'Agnol, R., Oliveira, M.A., Almeida, J.A.C., Althoff, F.J., Leite, A.A.S., Oliveira, D.C., Barros, C.E.M., 2006. Archean and paleoproterozoic granitoids of the Carajás metallogenic province, eastern Amazonian craton. In: Dall'Agnol, R., Rosa-Costa, L. T., Klein, E.L. (Eds.), *Symposium on Magmatism, Crustal Evolution, and*

- Metallogenesis of the Amazonian Craton. Volume and Field Trip Guide. Belém, PRONEX-UFPA/BGNO, pp. 99–150.
- Day, R., Fuller, M., Schmidt, V.A., 1977. Hysteresis properties of titanomagnetites: grain size and compositional dependence. *Phys. Earth Planet. Inter.* 13 (4), 260–267. [https://doi.org/10.1016/0031-9201\(77\)90108-X](https://doi.org/10.1016/0031-9201(77)90108-X).
- de Kock, Michiel O., Evans, David A.D., Beukes, Nicolas J., 2009. Validating the existence of Vaalbara in the Neoproterozoic. *Precambrian Res.* 174 (1–2), 145–154. <https://doi.org/10.1016/j.precamres.2009.07.002>.
- Denyszyn, S.W., Feinberg, J.M., Renne, P.R., Scott, G.R., 2013. Revisiting the age and paleomagnetism of the Modipe Gabbro of South Africa. *Precambrian Res.* 238, 176–185. <https://doi.org/10.1016/j.precamres.2013.10.002>.
- Dreher, Ana M., Xavier, Roberto P., Taylor, Bruce E., Martini, Sérgio L., 2008. New geologic, fluid inclusion and stable isotope studies on the controversial Igarapé Bahia Cu-Au deposit, Carajás Province, Brazil. *Miner. Deposita* 43 (2), 161–184. <https://doi.org/10.1007/s00126-007-0150-6>.
- Dunlop, David J., 1983. Paleomagnetism of Archean rocks from northwestern Ontario: Wabigoon gabbro. Wabigoon Subprovince. *Can. J. Earth Sci.* 20 (12), 1805–1817. <https://doi.org/10.1139/e83-172>.
- Dunlop, D.J., Özdemir, Ö., 1997. *Rock Magnetism: Fundamentals and Frontiers* (572, pp.).
- Dunlop, D.J., 2002. Theory and application of the Day plot (Mrs/Ms versus Hcr/Hc) 1. Theoretical curves and tests using titanomagnetite data. *J. Geophys. Res.: Solid Earth* 107, B3. <https://doi.org/10.1029/2001JB000486>.
- Eriksson, P.G., Condie, K.C., 2014. Cratonic sedimentation regimes in the ca. 2450–2000Ma period: relationship to a possible widespread magmatic slowdown on Earth? *Gondwana Res.* 25 (1), 30–47. <https://doi.org/10.1016/j.gr.2012.08.005>.
- Ernst, R.E., 2014. *Large Igneous Provinces, 1–653*. Cambridge University Press, Cambridge.
- Ernst, R.E., Bleeker, W., 2010. Large igneous provinces (LIPs), giant dyke swarms, and mantle plumes: significance for breakup events within Canada and adjacent regions from 2.5 Ga to the present. *Can. J. Earth Sci.* 47, 695–739. <https://doi.org/10.1139/E10-025>.
- Ernst, Richard E., Buchan, Kenneth L., 2001. In: *Mantle plumes: their identification through time*. Geological Society of America. <https://doi.org/10.1130/0-8137-2352-3.483>.
- Ernst, R.E., Youbi, N., 2017. How Large igneous provinces affect global climate, sometimes cause mass extinctions, and represent natural markers in the geological record. *Palaeogeography, Palaeoclimatology, Palaeoecology* 478, 30–52. <https://doi.org/10.1016/j.palaeo.2017.03.014>.
- Ernst, R.E., Bond, D.P.G., Zhang, S.-H., Buchan, K.L., Grasby, S.E., Youbi, N., El Bilali, H., Bekker, A. and Doucet, L.S., 2021. Large Igneous Province Record Through Time and Implications for Secular Environmental Changes and Geological Time-Scale Boundaries. In *Large Igneous Provinces* (eds. R.E. Ernst, A.J. Dickson and A. Bekker). <https://doi.org/10.1002/9781119507444.ch1>.
- Evans, D.A.D., 2013. Reconstructing pre-Pangean supercontinents. *Geol. Soc. Am. Bull.* 125 (11–12), 1735–1751. <https://doi.org/10.1130/B30950.1>.
- Evans, D.A.D., Li, Z.X., Murphy, J.B., 2016. Four-dimensional context of Earth's supercontinents. *Geological Society, London, Special Publications* 424 (1), 1–14. <https://doi.org/10.1144/SP424.12>.
- Evans, D.A.D., Smirnov, A.V., Gumsley, A.P., 2017. Paleomagnetism and U-Pb geochronology of the Black Range dykes, Pilbara Craton, Western Australia: a Neoproterozoic crossing of the polar circle. *Australian Journal of Earth Sciences* 64 (2), 225–237. <https://doi.org/10.1080/08120099.2017.1289981>.
- Evans, M.E., Wayman, M.L., 1974. An investigation of the role of ultra-fine titanomagnetite intergrowths in paleomagnetism. *Geophys. J. Int.* 36, 1–10. <https://doi.org/10.1111/j.1365-246X.1974.tb03621.x>.
- Evans, Michael E., Muxworthy, Adrian R., 2019. Vaalbara paleomagnetism. *Can. J. Earth Sci.* 56 (9), 912–916. <https://doi.org/10.1139/cjes-2018-0081>.
- Feio, G.R.L., Dall'Agnol, R., Dantas, E.L., Macambira, M.J.B., Santos, J.O.S., Althoff, F.J., Soares, J.E.B., 2013. Archean granitoid magmatism in the Canaã dos Carajás area: implications for crustal evolution of the Carajás province, Amazonian craton, Brazil. *Precambrian Res.* 227, 157–185. <https://doi.org/10.1016/j.precamres.2012.04.007>.
- Ferreira Filho, C.F., Cançado, F., Correa, C., Macambira, E.M.B., Siepierski, L., Brod, T.C. J., 2007. Mineralizações estratiformes de EGP-Ni associadas a complexos acamadados em Carajás: os exemplos de Luanga e Serra da Onça. *Publicat. Gráfica & Editora, Contribuições à Geologia da Amazônia* 5, 01–14 (in Portuguese).
- Figueiredo e Silva, Rosaline C., Lobato, Lydia M., Zucchetti, Marcia, Hagemann, Steffen, Vennemann, Torsten, 2020. Geotectonic signature and hydrothermal alteration of metabasalts under- and overlying the giant Serra Norte iron deposits, Carajás mineral Province. *Ore Geology Reviews* 120, 103407. <https://doi.org/10.1016/j.oregeorev.2020.103407>.
- Fisher, R., 1953. Dispersion on a sphere. *Proc. R. Soc. Lond. A* 217 (1130), 295–305. <https://doi.org/10.1098/rspa.1953.0064>.
- Galarza, Marco Antonio, Macambira, Moacir José B., Villas, Raimundo Neto, 2008. Dating and isotopic characteristics (Pb and S) of the Fe oxide-Cu-Au-U-REE Igarapé Bahia ore deposit, Carajás mineral province, Pará state, Brazil. *J. S. Am. Earth Sci.* 25 (3), 377–397. <https://doi.org/10.1016/j.jsames.2007.07.006>.
- Gerya, T., 2019. Geodynamics of the early Earth: Quest for the missing paradigm. *Geology* 47, 1006–1007. <https://doi.org/10.1130/focus102019.1>.
- Gibbs, A.K., Wirth, K.R., Hirata, W.K., Olszewski Jr., W.J., 1986. Age and composition of the Grão Pará Group volcanics, Serra dos Carajás. *Revista Brasileira de Geociências* 16, 201–211.
- Gumsley, A.P., 2017. Validating the existence of the supercraton Vaalbara in the Mesoproterozoic to Palaeoproterozoic. Doctoral dissertation, Lithosphere and Biosphere Science, Department of Geology, Lund University. Litholund theses 30, 130.
- Gumsley, Ashley P., Chamberlain, Kevin R., Bleeker, Wouter, Söderlund, Ulf, de Kock, Michiel O., Larsson, Emilie R., Bekker, Andrey, 2017. Timing and tempo of the Great Oxidation Event. *Proc. Natl. Acad. Sci. U. S. A.* 114 (8), 1811–1816. <https://doi.org/10.1073/pnas.1608824114>.
- Hale, C.J., Lloyd, P., 1990. *Paleomagnetic Analysis of Regional and Contact Strains*. Ontario Geol. Surv. Misc. Paper. 150, 97–106.
- Halls, H.C., 1978. The use of converging remagnetization circles in palaeomagnetism. *Phys. Earth Planet. Inter.* 16 (1), 1–11. [https://doi.org/10.1016/0031-9201\(78\)90095-X](https://doi.org/10.1016/0031-9201(78)90095-X).
- Halla, J., Whitehouse, M.J., Ahmad, T., Bagai, Z., 2017. Archean granitoids: an overview and significance from a tectonic perspective. In: Halla, J., Whitehouse, M. J., Ahmad, T., Bagai, Z. (eds). *Crust–Mantle Interactions and Granitoid Diversification: Insights from Archean Cratons*. Geological Society, London, Special Publications, 449, pp. 1–18. <https://doi.org/10.1144/SP449.10>.
- Hawkesworth, C.J., Cawood, P.A., Dhuime, B., 2020. The Evolution of the Continental Crust and the Onset of Plate Tectonics. *Frontiers. Earth Science* 8 (326). <https://doi.org/10.3389/feart.2020.00326>.
- Holdsworth, R.E., Pinheiro, R.V.L., 2000. The anatomy of shallow-crustal transpressional structures: insights from the Archean Carajás fault zone, Amazon, Brazil. *Journal of Structural Geology* 22, 1105–1123. [https://doi.org/10.1016/S0191-8141\(00\)00036-5](https://doi.org/10.1016/S0191-8141(00)00036-5).
- Hrouda, F., 1994. A technique for the measurement of thermal changes of magnetic susceptibility of weakly magnetic rocks by the CS-2 Apparatus and KLY-2 Kappabridge. *Geophys. J. Int.* 118, 604–612. <https://doi.org/10.1111/j.1365-246X.1994.tb03987.x>.
- Kirschvink, J.L., 1980. The least-squares line and plane and the analysis of palaeomagnetic data. *Geophys. J. Int.* 62 (3), 699–718. <https://doi.org/10.1111/gji.1980.62.issue-310.1111/j.1365-246X.1980.tb02601.x>.
- Kirschvink, Joseph L., Kopp, Robert E., Raub, Timothy D., Baumgartner, Christopher T., Holt, John W., 2008. Rapid, precise, and high-sensitivity acquisition of paleomagnetic and rock-magnetic data: Development of a low-noise automatic sample changing system for superconducting rock magnetometers. *Geochemistry Geophysics. Geosys.* 9 (5), n/a–n/a. <https://doi.org/10.1029/2007GC001856>.
- Koymans, Mathijs R., Langereis, Cor G., Pastor-Galán, Daniel, van Hinsbergen, Douwe J. J., 2016. Paleomagnetism.org: An online multi-platform open source environment for paleomagnetic data analysis. *Comput. Geosci.* 93, 127–137. <https://doi.org/10.1016/j.cageo.2016.05.007>.
- Krymsky, R.S., Macambira, J.B., Macambira, M.J.B., 2002. Geocronologia U-Pb em zircão de rochas vulcânicas da Formação Carajás, Estado do Pará. In: *Simpósio Sobre Vulcanismo e Ambientes Associados*, 2, Belém, Anais. Belém, 41p. (in Portuguese).
- Kumar, A., Parashuramulu, V., Shankar, R., Besse, J., 2017. Evidence for a Neoproterozoic LIP in the Singhbhum craton, eastern India: Implications to Vaalbara supercontinent. *Precambrian Res.* 292, 163–174. <https://doi.org/10.1016/j.precamres.2017.01.018>.
- Lacasse, Christian Michel, Ganade, Carlos Eduardo, Mathieu, Lucie, Teixeira, Novevaldo Araújo, Lopes, Leonardo Brenguer Leão, Monteiro, Cimara Francisca, 2020. Restoring original composition of hydrothermally altered Archean metavolcanic rocks of the Carajás Mineral Province (Brazil): Geodynamic implications for the transition from lid to mobile tectonics. *Lithos* 372–373, 105647. <https://doi.org/10.1016/j.lithos.2020.105647>.
- Liu, Y., Mitchell, R.N., Li, Z.X., Kirscher, U., Pisarevsky, S.A., Wang, C., 2021. Archean geodynamics: Ephemeral supercontinents or long-lived supercratons. *Archean geodynamics: Ephemeral supercontinents or long-lived supercratons. Geology* 49, G48575.1. <https://doi.org/10.1130/G48575.1>.
- Lubnina, N.V., Slabunov, A.I., 2009. Paleomagnetism in the Neoproterozoic Polyphase Panozero Intrusion in the Fennoscandian Shield. *Mosc. Univ. Geol. Bull.* 64 (6), 346–353. <https://doi.org/10.3103/S0145575209060039>.
- Macambira, J.B., 2003. O ambiente deposicional da Formação Carajás e uma proposta de modelo evolutivo para a Bacia Grão Pará (Unpublish Ph.D. Thesis), Instituto de Geociências, Universidade Estadual de Campinas, pp. 217.
- Machado, N., Lindenmayer, Z., Krogh, T.E., Lindenmayer, D., 1991. U-Pb geochronology of Archean magmatism and basement reactivation in the Carajás area, Amazon shield. *Brazil. Precambrian Res.* 49 (3–4), 329–354. [https://doi.org/10.1016/0301-9268\(91\)90040-H](https://doi.org/10.1016/0301-9268(91)90040-H).
- Martins, P.L.G., Toledo, C.L.B., Silva, A.M., Chemale Jr., F., Santos, J.O.S., Assis, L.M., 2017. Neoproterozoic magmatism in the southeastern Amazonian Craton, Brazil: petrography, geochemistry and tectonic significance of basalts from the Carajás Basin. *Precambrian Res.* 302, 340–357. <https://doi.org/10.1016/j.precamres.2017.10.013>.
- McFadden, P.L., McElhinny, M., 1990. Classification of the reversal test in palaeomagnetism. *Geophys. J. Int.* 103, 725–729. <https://doi.org/10.1111/j.1365-246X.1990.tb05683.x>.
- Meert, J.G., Pivarunas, A.F., Evans, D.A.D., Pisarevsky, S.A., Pesonen, L.J., Li, Z., Elming, S., Miller, S.R., Zhang, S., Salminen, J.M., 2020. The magnificent seven: A proposal for modest revision of the Van der Voo (1990) quality index. *Tectonophysics* 790, 228549. <https://doi.org/10.1016/j.tecto.2020.228549>.
- Meirelles, M.R., Dardenne, M.A., 1991. Vulcanismo basáltico de afinidade shoshonítica e ambiente de arco arqueano, Grupo Grão-Pará, Serra dos Carajás, Pará. *Revista Brasileira de Geociências* 21, 41–50 (in Portuguese).
- Mitchell, Ross N., Zhang, Nan, Salminen, Johanna, Liu, Yebo, Spencer, Christopher J., Steinberger, Bernhard, Murphy, J. Brendan, Li, Zheng-Xiang, 2021. The supercontinent cycle. *Nat Rev Earth Environ* 2 (5), 358–374. <https://doi.org/10.1038/s43017-021-00160-0>.
- Moreto, Carolina P.N., Monteiro, Lena V.S., Xavier, Roberto P., Creaser, Robert A., DuFrane, S. Andrew, Melo, Gustavo H.C., Delnardo da Silva, Marco A., Tassinari, Colombo C.G., Sato, Kei, 2015. Timing of multiple hydrothermal events in the iron oxide–copper–gold deposits of the Southern Copper Belt, Carajás Province.

- Brazil. *Miner. Deposita* 50 (5), 517–546. <https://doi.org/10.1007/s00126-014-0549-9>.
- Morrison, D.A., Davis, D.W., Wooden, J.L., Bogard, D.D., Maczuga, D.E., Phinney, W.C., Ashwal, L.D., 1985. Age of the Mulcahy Lake intrusion, northwest Ontario, and implications for the evolution of greenstone-granite terrains. *Earth Planet. Sci. Lett.* 73 (2–4), 306–316. [https://doi.org/10.1016/0012-821X\(85\)90079-2](https://doi.org/10.1016/0012-821X(85)90079-2).
- Müller, R., Dietmar, Cannon, John, Qin, Xiaodong, Watson, Robin J., Gurnis, Michael, Williams, Simon, Pfaffelmoser, Tobias, Seton, Maria, Russell, Samuel H.J., Zahirovic, Sabin, 2018. GPlates: Building a virtual Earth through deep time. *Geochemistry, Geophysics, Geosystems* 19 (7), 2243–2261. <https://doi.org/10.1029/2018GC007584>.
- Nesse, William D., 2000. *Introduction to mineralogy*. Oxford University Press, New York, p. 361.
- Olsson, J.R., Söderlund, U., Klausen, M.B., Ernst, R.E., 2010. U-Pb baddeleyite ages linking major Archean dyke swarms to volcanic-rift forming events in the Kaapvaal craton (South Africa), and a precise age for the Bushveld Complex. *Precambrian Res.* 183 (3), 490–500. <https://doi.org/10.1016/j.precamres.2010.07.009>.
- OLSZEWSKI, W., WIRTH, K., GIBBS, A., GAUDETTE, H., 1989. The age, origin, and tectonics of the Grão Pará Group and associated rocks, Serra dos Carajás, Brazil: Archean continental volcanism and rifting. *Precambrian Res.* 42 (3–4), 229–254. [https://doi.org/10.1016/0301-9268\(89\)90013-2](https://doi.org/10.1016/0301-9268(89)90013-2).
- Palin, Richard M., Santosh, M., Cao, Wentao, Li, Shan-Shan, Hernández-Urbe, David, Parsons, Andrew, 2020. Secular change and the onset of plate tectonics on Earth. *Earth Sci. Rev.* 207, 103172. <https://doi.org/10.1016/j.earscirev.2020.103172>.
- Pesonen, L.J., Elming, S.-Å., Mertanen, S., Pisarevsky, S., D'Agrella-Filho, M.S., Meert, J. G., Schmidt, P.W., Abrahamsen, N., Bylund, G., 2003. Palaeomagnetic configuration of continents during the Proterozoic. *Tectonophysics* 375 (1–4), 289–324. [https://doi.org/10.1016/S0040-1951\(03\)00343-3](https://doi.org/10.1016/S0040-1951(03)00343-3).
- Pivarnunas, A.F., Meert, J.G., Miller, S.R., 2018. Assessing the intersection/remagnetization puzzle with synthetic apparent polar wander paths. *Geophys. J. Int.* 214, 1164–1172. <https://doi.org/10.1093/gji/ggy216>.
- Planavsky, Noah J., Crowe, Sean A., Fakrae, Mojtaba, Beaty, Brian, Reinhard, Christopher T., Mills, Benjamin J.W., Holstege, Cerys, Konhauser, Kurt O., 2021. Evolution of the structure and impact of Earth's biosphere. *Nat Rev Earth Environ* 2 (2), 123–139. <https://doi.org/10.1038/s43017-020-00116-w>.
- Rapalini, A.E., Luppo, T., Llanos, M.P.I., Vásquez, C.A., Valencio, L.D.P.D.A., 2013. Successful paleomagnetic azimuthal orientation of drill cores from a hydrocarbon source rock reservoir: the case of the Vacca Muerta Formation, Neuquén Basin, Argentina. *Latinmag Letters*, 3, Special Issue, 1–5.
- Reddy, S.M., Evans, D.A.D., 2009. Palaeoproterozoic supercontinents and global evolution: correlations from core to atmosphere. *Geol. Soc. Spec. Pub.* 323 (1), 1–26. <https://doi.org/10.1144/SP323.1>.
- Rolph, T.C., Shaw, J., Harper, T.R., Hagan, J.T., 1995. Viscous remanent magnetization: a tool for orientation of drill cores. *Geological Society, London, Special Publications* 98 (1), 239–243. <https://doi.org/10.1144/GSL.SP.1995.098.01.14>.
- Rosière, C.A., Baars, F.J., Seoane, J.C.S., Lobato, L.M., Silva, L.L., Mendes, G.E., 2006. Structure and iron mineralization of the Carajás province. *B. Appl. Earth Sci.* 115 (4), 126–133. <https://doi.org/10.1179/174327506X138986>.
- Rosignol, Camille, Siciliano Rego, Eric, Narduzzi, Francesco, Teixeira, Lívia, Ávila, Janaína N., Silva, Marco A.L., Lana, Cristiano, Philippot, Pascal, 2020. Stratigraphy and geochronological constraints of the Serra Sul Formation (Carajás Basin, Amazonian Craton, Brazil). *Precambrian Res.* 351, 105981. <https://doi.org/10.1016/j.precamres.2020.105981>.
- Rosignol, Camille, Antonio, Paul Yves Jean, Narduzzi, Francesco, Rego, Eric Siciliano, Teixeira, Lívia, de Souza, Romário Almeida, Ávila, Janaína N., Silva, Marco A.L., Lana, Cristiano, Trindade, Ricardo I.F., Philippot, Pascal, 2021. Unraveling one billion years of geological evolution of the southeastern Amazonia Craton from detrital zircon analyses. *Geoscience Frontiers* (in press) 101202. <https://doi.org/10.1016/j.gsf.2021.101202>.
- Salminen, J., Oliveira, E.P., Piispa, E.J., Smirnov, A.V., Trindade, R.I.F., 2019. Revisiting the paleomagnetism of the Neoproterozoic Uauá mafic dyke swarm, Brazil: Implications for Archean supercratons. *Precambrian Res.* 329, 108–123. <https://doi.org/10.1016/j.precamres.2018.12.001>.
- Schmidt, P.W., Embleton, B.J.J., 1985. Prefolding and overprint magnetic signatures in Precambrian (c.2.9–2.7 Ga) igneous rocks from the Pilbara craton and Hamersley Basin, NW Australia. *J. Geophys. Res.* 90, 2967–2984. <https://doi.org/10.1029/JB090IB04p02967>.
- Sergeyev, S.A., Lobach-Zhuchenko, S.B., Larionov, A.N., Berezhnaya, N.G., Guseva, N.S., 2007. Archean age of miaskite lamproites from the Panozero complex, Karelia. *Dokl. Earth Sci.* 413, 420–423. <https://doi.org/10.1134/S1028334X07030221>.
- Smirnov, A.V., Evans, D.A.D., Ernst, R.E., Söderlund, U., Li, Z.-X., 2013. Trading partners: Tectonic ancestry of southern Africa and western Australia, in Archean supercratons Vaalbara and Zimgarn. *Precambrian Res.* 224, 11–22. <https://doi.org/10.1016/j.precamres.2012.09.020>.
- Strik, G., Blake, T.S., Zegers, T.E., White, S.H., Langereis, C.G., 2003. Palaeomagnetism of flood basalts in the Pilbara Craton, Western Australia: Late Archean continental drift and the oldest known reversal of the geomagnetic field. *Journal of Geophysical Research, Solid Earth* 108, 1–21. <https://doi.org/10.1029/2003JB002475>.
- Tallarico, F.H.B., Figueiredo, B.R., Groves, D.I., Kositcin, N., McNaughton, N.J., Fletcher, I.R., Rego, J.L., 2005. Geology and SHRIMP U-Pb geochronology of the Igarapé Bahia deposit, Carajás copper-gold belt, Brazil: an Archean (2.57 Ga) example of iron-oxide Cu-Au-(U-REE) mineralization. *Econ. Geol.* 100, 7–28. <https://doi.org/10.2113/100.1.0007>.
- Tauxe, L., Watson, G.S., 1994. The fold test: an eigen analysis approach. *Earth Planet. Sci. Lett.* 122 (3–4), 331–341. [https://doi.org/10.1016/0012-821X\(94\)90006-X](https://doi.org/10.1016/0012-821X(94)90006-X).
- Tavares, F.M., Trouw, R.A.J., da Silva, C.M.G., Justo, A.P., Oliveira, J.K.M., 2018. The multistage tectonic evolution of the northeastern Carajás Province, Amazonian Craton, Brazil: Revealing complex structural patterns. *J. S. Am. Earth Sci.* 88, 238–252. <https://doi.org/10.1016/j.jsames.2018.08.024>.
- Teixeira, J.B.G., Eggler, D.H., 1994. Petrology, geochemistry, and tectonic setting of Archean basaltic and dioritic rocks from the N4 iron deposit, Serra dos Carajás, Pará, Brazil. *Acta Geol. Leopoldensia* 17, 71–114.
- Teixeira, Novaldo Araújo, Campos, Leandro Duarte, Paula, Rodolfo Reis de, Lacasse, Christian Michel, Ganade, Carlos Eduardo, Monteiro, Cimara Francisca, Lopes, Leonardo Brenguere Leão, Oliveira, Claudinei Gouveia de, 2021. Carajás Mineral Province - Example of metallogeny of a rift above a cratonic lithospheric keel. *J. S. Am. Earth Sci.* 108, 103091. <https://doi.org/10.1016/j.jsames.2020.103091>.
- Teixeira, W., Hamilton, M., Girardi, V.A.V., Faleiros, F.M., Ernst, R.E., 2019. U-Pb baddeleyite ages of key dyke swarms in the Amazonian Craton (Carajás/Rio Maria and Rio Apa areas): tectonic implications for events at 1880, 1110 Ma, 535 Ma and 200 Ma. *Precambrian Res.* 329, 138–155. <https://doi.org/10.1016/j.precamres.2018.02.008>.
- Trendall, A.F., 1968. Three great basins of Precambrian iron formation deposition: a systematic comparison. *Geol. Soc. Am. Bull.* 79, 1527–1533. [https://doi.org/10.1130/0016-7606\(1968\)79\[1527:TGBOPB\]2.0.CO;2](https://doi.org/10.1130/0016-7606(1968)79[1527:TGBOPB]2.0.CO;2).
- Trendall, A.F., Basei, M.A.S., de Laeter, J.R., Nelson, D.R., 1998. SHRIMP zircon U-Pb constraints on the age of the Carajás Formation, Grão Pará Group, Amazon Craton. *J. S. Am. Earth Sci.* 11 (3), 265–277. [https://doi.org/10.1016/S0895-9811\(98\)00015-7](https://doi.org/10.1016/S0895-9811(98)00015-7).
- Van Kranendonk J., M., Hickman H., A., Smithies H., R., Williams R., I., Bagas, L., Farrell R., T., 2006. Revised lithostratigraphy of Archean supracrustal and intrusive rocks in the northern Pilbara Craton, Western Australia. *Western Australia Geological Survey* 15, 57pp.
- Vasquez, M.L., Carvalho, J.M.A., Sousa, C.S., Ricci, P.S.F., Macabira, E.M.B., Costa, L.T.R., 2008. Mapa Geológico do Pará em SIG. Brazilian Geological Survey – CPRM.
- Williams, Harold, Hoffman, Paul F., Lewry, John F., Monger, James W.H., Rivers, Toby, 1991. Anatomy of North America: thematic geologic portrayals of the continent. *Tectonophysics* 187 (1–3), 117–134. [https://doi.org/10.1016/0040-1951\(91\)90416-P](https://doi.org/10.1016/0040-1951(91)90416-P).
- Windley, Brian F., Kusky, Tim, Polat, Ali, 2021. Onset of plate tectonics by the Eoarchean. *Precambrian Res.* 352, 105980. <https://doi.org/10.1016/j.precamres.2020.105980>.
- Wingate, M.T.D., 1998. A palaeomagnetic test of the Kaapvaal-Pilbara (Vaalbara) connection at 2.78 Ga. *South African J. Geol.* 101, 257–274.
- Zhang, C.L., Ye, X.T., Ernst, R.E., Zhong, Y., Zhang, J., Li, H.K., Long, X.P., 2019. Revisiting the Precambrian evolution of the Southwestern Tarim Terrane: implication for its role in Precambrian supercontinents. *Precambrian Res.* 324, 18–31. <https://doi.org/10.1016/j.precamres.2019.01.018>.
- Zijderveld, J., 1967. AC demagnetization of rocks: analysis of results. *Methods Paleomagn.* 3, 254.
- Zucchetti, M., 2007. Rochas máficas do Supergrupo Grão Pará e sua relação com a mineralização de ferro dos depósitos N4 e N5, Carajás, PA: Unpublished Ph.D. thesis, Belo Horizonte, Brazil, Universidade Federal de Minas Gerais, 125 p (in Portuguese).